scientific reports

Check for updates

OPEN

Conserved regions and molecular cloning of *Acid* and *Alkaline phosphatases* in *Streptomyces* sp. MMA-NRC

Nagwa M. Abd El-Aziz[1,2]✉

Phosphorus is one of the most important nutrients for the growth and development of plants. Although chemical fertilizers supply phosphorus, much of it remains in insoluble forms inaccessible to plants. Numerous applications exist for phosphate-solubilizing bacteria as biological fertilizers in agriculture. By employing sustainable agricultural practices, the use of biofertilizers rather than artificial fertilizers can reduce environmental contamination and increase crop productivity. Here, we explored conserved regions and the gene encoding *acid phosphatase* (*ACPase*) and *alkaline phosphatase* (*ALPase*) sequences from *Streptomyces sp. MMA-NRC*, the specimen was separated; genes were sequenced, annotated, and officially recorded in the NCBI GenBank database with unique identification numbers PV646716 and PV646717. Ramachandran's plot was used to validate the 3D structure of the simulated *ACPase* and *ALPase* proteins. The results showed that a significant portion of the amino acid residues were located in the most favored region for the strain *Streptomyces NM-NRC*, which revealed that 488 and 560 residues, accounting for 94.37 and 93.08% overall quality factor for *ACPase* and *ALPase; respectively.* strain 4 F and strain *Streptomyces sp. MMA-NRC.* Docking studies revealed optimal binding affinities of the *ACPase* and *ALPase* proteins with rock phosphate, with high affinity scores for the strain *Streptomyces sp. MMA-NRC*. Which recorded an affinity score of -110.86 kcal/mol, a confidence score of 0.3137, a ligand RSMD (Å) of 69.31, for wild type strain *Streptomyces* sp. MMA-NRC *ACPase*. In addition, recorded affinity score of – 108.55 kcal/mol, confidence score of 0.3039, ligand RSMD (Å) of 33.68, for the wild type strain *Streptomyces* sp. MMA-NRC *ALPase* strain. Molecular cloning and expression of the *Streptomyces sp. MMA-NRC ACPase* and *ALPase* genes in *E. coli DH5α* resulted in a recombinant *E. coli DH5α* pGEM-*T-ACPase* and *E. coli DH5α* pGEM-*T-ALPase* significantly higher available phosphore using ascorbic acid colorimetric method of 52.64 and 57.22 mg/L^{-1}; respectively after 7 days of incubation, compared to the wild type *Streptomyces sp. MMA-NRC*, which exhibited a value 35.44 mg/L^{-1} after 7 days of incubation. These results suggest that the use of *Streptomyces sp. MMA-NRC* for phosphatase production seems to be very promising since it has a diverse array of agricultural uses, including plant biofertilizers.

Keywords Acid phosphatase, Alkaline phosphatase, Streptomyces sp., Rock phosphate, Modeled structure 3D, Molecular docking, Molecular cloning

Second only to nitrogen, phosphorus is a crucial macronutrient for plants. It is directly involved in the synthesis of nucleic acids, cell division, and the development of new tissues. It is also required for a number of cellular functions, including photosynthesis, energy production, carbohydrate metabolism, redox homeostasis, and signaling[1–3]. Phosphorus is also necessary for plant growth and development; levels can reach 0.2% of the dry weight of plants[4]. However, arable land around the world has more total phosphorus and less available phosphorus, and the concentration of plant-available phosphorus rarely surpasses 10 µM, which has a significant impact on agricultural development and plant growth[5]. Thirty to sixty-five% of soil phosphorus is organic, and the remaining thirty to seventy% is inorganic. Long-term application of phosphorus fertilizer overwhelmingly produces phosphate that is difficult for plants to directly absorb and cannot fully address phosphorus deficiencies in soils because organic phosphorus typically exists in the soil in an inert form and is fixed to form insoluble

[1]Microbial Genetic Department, Biotechnology Research Institute, National Research Centre, 33 El Buhouth ST, Dokki, Cairo 12622, Egypt. [2]Dokki, Giza, Egypt. ✉email: nagwamkh@gmail.com

phosphorus forms, which are difficult for plants to directly absorb and use, and inorganic phosphorus readily reacts with ions in the soil, such as Fe3+, Al3+, and Ca2+ [6,7].

In an effort to increase crop productivity, farmers frequently apply excessive amounts of fertilizer. Over application of fertilizer can result from erroneous perceptions about its efficacy. A common misconception is that increased fertilizer equals increased output. This problem is additionally exacerbated by inadequate soil testing and knowledge[8], furthermore, some people can continue to use antiquated methods without taking into account the particular nutrient requirements of their crops. Sometimes there is a lack of trustworthy information, which leads to bad decisions. Farmers who are under pressure to satisfy consumer demands may put short-term outcomes ahead of long-term strategies. Excessive use of phosphate and nitrogen fertilizers can cause eutrophication, imbalances in soil nutrients, and adverse effects on the food chain. When fertilizers are utilized excessively, nutrient contamination becomes a serious issue. Runoff from agriculture can cause this kind of contamination by introducing phosphorus and nitrogen into streams. This type of drainage causes toxic algal blooms. Toxins produced by these blooms pose a risk to aquatic ecosystems and public health. Hypoxia, or low oxygen levels, are also caused by the decomposition and death of algae, which uses up oxygen in the water. These circumstances make it difficult for fish and other marine life to survive, which frequently leads to die-offs. Therefore, one of the main causes of nutrient contamination in agriculture is the overuse of nutrients, especially nitrogen and phosphorus. The main cause of this problem is agricultural runoff, which occurs when fertilizers used on crops wash into adjacent streams during irrigation or rainfall. Both freshwater and marine ecosystems are impacted by such nutrient overload, which causes major problems with water quality. Additionally, overuse of phosphate fertilizers may cause the microbiological ecology in the soil to be destroyed. Furthermore, the overabundance of nutrients upsets the environment's natural equilibrium, which results in a decline in biodiversity. Nutrient imbalances cause the health of the soil to deteriorate, which might damage beneficial microbes that are necessary for successful farming. Concerns about climate change may worsen if greenhouse gas emissions rise.

The world's phosphate supplies are finite and will likely run out in 50–100 years, or roughly 2059–2109[9]. There are currently an estimated 370 years of globally reserves left at current extraction rates, up from less than 100 years with earlier estimates due to significant improvements in the USGS's phosphate rock reserve estimations in 2011. These reserves are geographically concentrated, with Morocco alone controlling around three-quarters of them. Output is similarly notably concentrated, with two-thirds of output coming from three countries: China, the US, and Morocco. The current disparity in reserve-to-production (R/P) ratios among nations is probably going to change how reserves and production are distributed in the future. According to the analysis, reserves may last 300–400 years globally, but most nations will have used them up in 100 years, leaving a significant output shortfall. Morocco's R/P ratio of almost 2000 years significantly distorts the worldwide figure. Since more than 70% of world output is now produced in nations with R/P ratios under 100 years, the depletion of these reserves would cause a significant production deficit of about 125 Mt year in the twenty-first century. Together, China and the US produce more than half of the world's current supply, and at present extraction rates, both will run out in 60 years. The future production landscape will therefore be significantly altered as merely maintaining present levels of production will require large increases in production within some counties to balance depletion within others[10], the projected production shortfall will be exacerbated by the growing demand for phosphate rock. Future demand for phosphate rock is probably going to be significantly higher due to growing populations and the per capita need for phosphorus. The demand for phosphate rock is projected to rise at a 1% annual rate from 2010 to 2050, reaching 262 Mt, and then leveling out at 0% by 2050, causing a production deficit by 2075. Morocco's share of world production is projected to rise from 15% in 2010 to nearly 40% in 2050 and 80% in 2100, despite slow depletion of reserves and its largest R/P ratio.In conclusion, Morocco's monopoly on phosphate rock stocks and production is posing geopolitical risks, increasing dependence on one nation for vital resources. Prioritizing a food-production system that improves phosphorus use efficiency and recycles phosphorus-containing waste is crucial for future phosphorus and food security.

However, as new phosphate ores have lately been found in Scandinavian nations like Norway, these statistics may need to be updated. Finding alternate, economically feasible, and environmentally acceptable methods to raise phosphorus levels in low-phosphorus or phosphorus-deficient soils for plant growth is necessary due to the negative effects of applying phosphorus fertilizers and the decrease in global phosphorus stocks[1]. Phosphate solubilizing bacteria (PSB), which play a crucial role in the soil phosphorus cycle by hydrolyzing inorganic phosphorus minerals through enzyme activity and mineralizing organic phosphorus through acid secretion, provide a biological solution to phosphorus deficiency in soils[11,12]. This increases the amount of available phosphorus in soils by solubilizing insoluble phosphorus. The ability of PSB to transform the insoluble phosphorus forms found in soils into accessible phosphorus that may be directly absorbed and used by plants through various pathways has been validated by a number of recent research. Examples include the production of dissolved phosphate by the release of enzymes (phytase and phosphatase), acids (organic and inorganic), and chelation (siderophores, extracellular polysaccharides)[12,13]. PSB can work in concert with phosphate fertilizers to promote phosphorus use in addition to their own capacity to change phosphorus speciation[14]. Additionally, PSB are progressively being used as raw materials for biofertilizers and inoculants; their application in agricultural fields has a notable impact and can greatly boost the productivity of agronomic crops in agro-ecological niches[15,16]. There are currently few thorough studies from several angles and a narrow focus on PSB gene regulation and phosphatase enzyme protein engineering processes. The ecological environment in soil is so complex that both the exogenous addition of PSB and fertilization will cause changes in microbial communities, which indirectly alter the phosphorus content in soil. PSB metabolites have varying levels of capacity due to the interference of PSB species and external factors, and many functional genes have different effects at different levels. Based on these results, the current study's objective was to evaluate the 3D structure of the simulated pho proteins using the genes encoding the sequences of *acid phosphatase* (*ACPase*) and *alkaline phosphatase*

(*ALPase*) from *Streptomyces sp*. MMA-NRC. The *ACPase* and *ALPase* proteins' ideal binding affinities with rock phosphate were found through docking studies. To increase phosphatase activity and accessible phosphorus, the *Streptomyces sp*. MMA-NRC *ACPase* and *ALPase* genes were molecularly cloned and expressed in *E. coli DH5α*.

Materials and methods

Plasmids, reagents, media and strains

Streptomyces sp. MMA-NRC (accession no. OR770185), as reported by[17], which might effectively solubilizing the rock phosphate (RP) was kept in our laboratory according to the specified instructions at -20 °C glycerol stocks. *E. coli DH5a* was cultivated at a temperature of 37 degrees Celsius for a duration of 12 to 18 h in either Luria-Bertani (LB) broth or low-salt LB medium. The following concentrations (g/L) are found in the National Botanical Research in P medium (NBRIP media), the basic medium used to isolate and ferment that solubilizes the rock phosphate[17,18]: glucose (10 g), $MgSO_4.7H_2O$ 0.25 g, $(NH_4)_2SO_4$ 0.1 g, KCl 0.2 g, and agar (15 g) supplemented with 5 g rock phosphate (RP) from Khouribga phosphate mine, pH 7, and agar 15 g.The rock phosphate is dissolved in 1,000 ml of distilled water[19]. They were cultured for three to seven days in orbital shaker (180 rpm) at 37 °C. For actinomycetes growth was used plate count (P.C.) agar medium (Himedia, West Chester, Pennsylvania, USA). Promega Co. in Madison, WI, USA, provided the plasmid known as pGEM-T Easy-cloning.It has 3015 base pairs and was manufactured by Amp^r. Both wild-type *Streptomyces sp.* has genomic DNA extracted. With the use of a genomic DNA isolation kit made in Taoyuan, Taiwan by GeneDireX, Inc. The plasmid DNA of *E. Coli DH5a* was extracted using the QIA prep spin miniprep kit. The T4 DNA ligase was supplied by TaKaRa in China and NEB in the US.

Quantitative estimation of available phosphorus solubilizing assessment using rock phosphate

The quantitative solubilization ability of RP by phosphate-solubilizing bacteria was tested in a liquid medium containing NBRIP. To do this, a pre culture in plate count medium was prepared overnight and subsequently transferred to NBRIP medium. For seven days of incubation at 37 °C with shaking at 150 rpm, 20 ml of the bacterial cultures were removed and centrifuged for fifteen minutes at 12,000xg. After being extracted, supernatants were measured for pH and their available P content, samples done in three replicates and take average of three replicates. The control treatments were administered without inoculation in the same way. The available phosphorus was measured spectrophotometrically in accordance with[20], and extracted using 0.5 M $NaHCO_3$ at pH 8.5[21]. The ascorbic acid colorimetric method was used to determine the as available P concentration[20]. After a few minutes of incubation at room temperature, around 1 mL of supernatant is combined with 160 µL of a reaction solution, and the optical density (OD) was measured at 880 nm using Shimadzu UV-visible spectrophotometer. The calculation of available phosphorus content was performed using a standard curve of KH_2PO_4 betewwn absorption at 880_{nm} and concentration, with calibration curve equation of: mg/kg^{-1}= (a-b)*(v*df*mcv/w) where: a = P concentration in extracted sample ($mg\ L^{-1}$), b = P concentration in the target ($mg\ L^{-1}$), V = extraction volume (mL), W = soil sample weight (g), DF = dilution factor = total solution volume/aliquot (extract) and mcf = humidity correction factor. $R^2 \geq 0.995$. Phosphate concentration was expressed in term of mg/L^{-1} phosphate released in culture.

Acid phosphatase (ACPase) and alkaline phosphatase (ALPase) encoding genes amplification

Initially, the product's design was determined by the DNA sequence of the primers intended for the *acid phosphatase (ACPase)* and *alkaline phosphatase* (*ALPase*) genes of *Streptomyces sp.* 4 F.Using a genomic DNA isolation kit (GeneDireX, Inc., Taoyuan, Taiwan), genomic DNA was recovered from the *Streptomyces sp*. MMA-NRC strain (NCBI Accession No. OR770185), as described by[17]. The *acid phosphatase* (*ACPase)* and *alkaline phosphatase* (*ALPase*) genes were amplified using the isolated material. The *ACPase* and *ALPase* gene DNA sequences of the *Streptomyces* sp. MMA-NRC strain were found to be significantly similar, leading to the development of particular primers. These primers designed using Primer3 based on conserved regions of *ACPase* and *ALPase* genes as follows: *ACPase*-F (5′- GAGGCGGACGGCGGG-3′) and the reverse primer *ACPase*-R (5′- CGAGGCGGCGGACAGTT-3′), and the forward primer *ALPase*-F (5′- TTCCTGCACGGCGTC GC – 3′) and the reverse primer *ALPase*-R (5′- GCGGGTGCGGTAGGAGC – 3′).The analysis revealed *ACPase* and *ALPase* genes have an open reading frame (ORF) of 1464 and 1680 bp, respectively. Using a GeneAmp PCR System 2400 heat cycler from PerkinElmer in Norwalk, Connecticut, USA, the PCR was performed using 100 ng of genomic DNA in a 100 µl reaction with 5 µM primers and master mix (TIANGEN, Beijing, China)[17]. The thermal protocol called for five minutes of denaturation at 95 °C, one minute of annealing at 57.5 °C, two minutes of extension at 72 °C per kilobase pair (kbp), and three minutes of extension at 72 °C. There were thirty-five cycles in all. The amplified genes were eluted using a FavorPrep gel purification kit (FAVORGEN, Biotech Corp., Ping Tung, Taiwan) prior to sequencing. The PCR results were then examined following electrophoresis on a 1% agarose gel and 10.000 bp DNA ladder (Invitrogen, California, USA), as shown in Fig. 1[22].

Bioinformatics analysis

The *ACPase* and *ALPase* protein sequences were obtained from the experimentally determined data *phosphatase* (*pho*) protein of *Streptomyces* sp. strain MMA-NRC using the online translation tool ExPASY (http://web.expasy.org/translate). The NCBI protein blast tool (BLAST: Basic Local Alignment Search Tool) was used to analyze the inferred amino acids. Blast performs duplicate-free searches of the protein sequence database, classifying finds containing identical sequences as matches[23,24]. The *ACPase* and *ALPase* protein's PDBsum home page (ebi.ac.uk) secondary structure prediction was performed using the online PDBsum tool[25]. Using the BLAST program, a cluster analysis (phylogenetic tree) of the wild-type *ACPase* and *ALPase* protein sequences were performed.

Homology modelling and validation of acid phosphatase (ACPase) and alkaline phosphatase (ALPase)

In order to forecast the tertiary configuration of *ACPase* and *ALPase* protein, ROBETTA (http://robetta.bakerlab.org) was used[26,27]. After five models were generated, the best model was determined by looking at the model with the highest confidence score (C-score, a statistic showing the correctness of the expected model)[28,29]. The C-score typically ranges from zero to one. An obvious relationship exists between the C-score and structural quality. Among the five generated models, an optimized *ACPase* and *ALPase* homology model was constructed using the "DOPE profile" options. The optimal validation framework for *ACPase* and *ALPase* proteins were verified using the SAVES v6.0 (structure analysis and verification server version 6) web tool (http://SAVESv6.0http://SAVESv6.0.ucla.edu - Structure Validation Server (ucla.edu) as well as the *ProSA* server. A total of five programs make up SAVES v6.0, and their purpose is to evaluate the protein structure's overall integrity. Subsequently, the model that was produced underwent evaluation using general stereo chemical parameters using the PROCHECK website. In addition, the *Ramachandran* plot was developed for the energy-minimized model of *ACPase* and *ALPase* structures. The x-axis of the plot is divided into four quadrants, which correspond to the low-energy area, permitted region, usually allowed region, and prohibited region[30], when amino acids located in allowed rejoin this indicated for high quality of protein model, but when amino acids located in disallowed rejoin this indicated for low or bad quality of protein model. Out of the five tools we employed, two stood out: VERIFY-3D, which analyzed the three-dimensional sequence profiles of protein models, and PROCHECK, which evaluated the structure using the Ramachandran plot[30,31]. Using the "PyMol" software developed by DeLano Scientific LLC, a stereo picture of the *ACPase* and *ALPase* models were created to display the surface groove structure[32].

Molecular docking studies

To process the 3D structure of the *ACPase* and *ALPase* proteins, the MOE program was used (Molecular Operating Environment (MOE) | MOEsaic | PSILO (chemcomp.com), Decanting the concentration of ions, water molecules, and present ligands. The receptor molecule was functionalized with hydrogen atoms by means of PyMOL (PyMOL | pymol.org). The rock phosphate ligand was created in pdb format using MOE and PyMOL; its PubChem SID is 459143506. The HDock online program was used to perform protein-ligand docking investigations (http://HDOCK.hust.edu.cn Server (hust.edu.cn)[30,33], in order to learn how rock phosphate interacts with *ACPase* and *ALPase*. Docking was the reason for saving the macromolecule file in PDB format[28,32,34], .

Preparation of competent cells methods

Competent cells were prepared from *E. coli DH5α* by using traditional $CaCl_2$ solution method of[35]. All preparations were performed in triplicates; all steps should be carried out on ice and eluted in 100 l of sterile Calcium Chloride Solutions. The quality of competent cells was assessed by calculating transformation efficiency[36,37].

Cloning and expression of acid phosphatase (ACPase) and alkaline phosphatase (ALPase) encoding genes

Using a kit from Promega Co., based in Madison, WI, USA, ligation cloning was performed using the amplified product *ACPase* and *ALPase* of *Streptomyces sp*. MMA-NRC, the pGEM®-T Easy cloning vector. The insert was inserted into the vector at the proper spots. The T4 ligase enzyme is used in a ligation process to create the recombinant plasmid. Twenty micrograms of ligated DNA and 0.1 millilitres of newly produced competent cells were mixed together; the transformation efficiency of the cells was $2.98*10^5$ colony-forming units per microgram of DNA[38]. After introducing the recombinant plasmid into *E. coli DH5a* cells using the heat shock protocol, the cells were incubated for one hour at 37 °C. After the incubation period, the samples were transferred onto LB agar plates that were enhanced with 40 µg X-gal, 50 µg/mL ampicillin, and 0.5 mM IPTG. Next, the plates were incubated at 37 °C for the entire night. The blue-white screening method was used to determine whether colonies were positive. *ACPase* and *ALPase* colonies were streaked once more on an appropriate plate that contained antibiotics, and they were thereafter incubated for 16 to 20 h at 37 degrees Celsius. In positive colonies, the extracellular expression of *ACPase* and *ALPase* activity was assessed using rock phosphate substrate at temperature 37 °C for seven days incubation[23,32,39,40]. After transforming *E. Coli DH5α* cells with plasmids *pGEM-T- ACPase* and *pGEM-T-ALPase*, overnight-grown single colonies were inoculated into Luria-Bertani (LB) broth medium supplemented with ampicillin (50 µg/mL) to create a 50 mL culture at OD_{600} harvest of the bacteria. After that, the culture was incubated for 16 h at 37 °C while being shaken. Centrifugation was applied to the mature culture for 10 min at 4 degrees Celsius, with a speed of 4000 revolutions per minute. Following the manufacturer's instructions, the liquid portion above the sediment cells was then removed, and the solid cell material was utilized to extract the plasmid DNA molecule[23]. Colony PCR screening was used to analyze the colonies that were transformed using the plasmid carrying the *ACPase* and *ALPase* genes (pGEM-T-), using specific primers for the *ACPase* and *ALPase* genes and the same PCR conditions as for amplifying these genes were part of this screening procedure.

Results and discussion

Acid phosphatase (ACPase) and alkaline phosphatase (ALPase) encoding genes amplification and alignment in Genbank (Blast)

In a previous study conducted by[17] actinomycetes *Streptomyces* sp. MMA-NRC strain was isolated and identified. The designed primers were for the *ACPase* and *ALPase* genes. The genes were successfully enhanced and sequenced. After that, we used BLAST to compare the obtained sequence to known sequences in the NCBI database. The analysis revealed *ACPase* and *ALPase* genes have an open reading frame (ORF) of 1464 and 1680

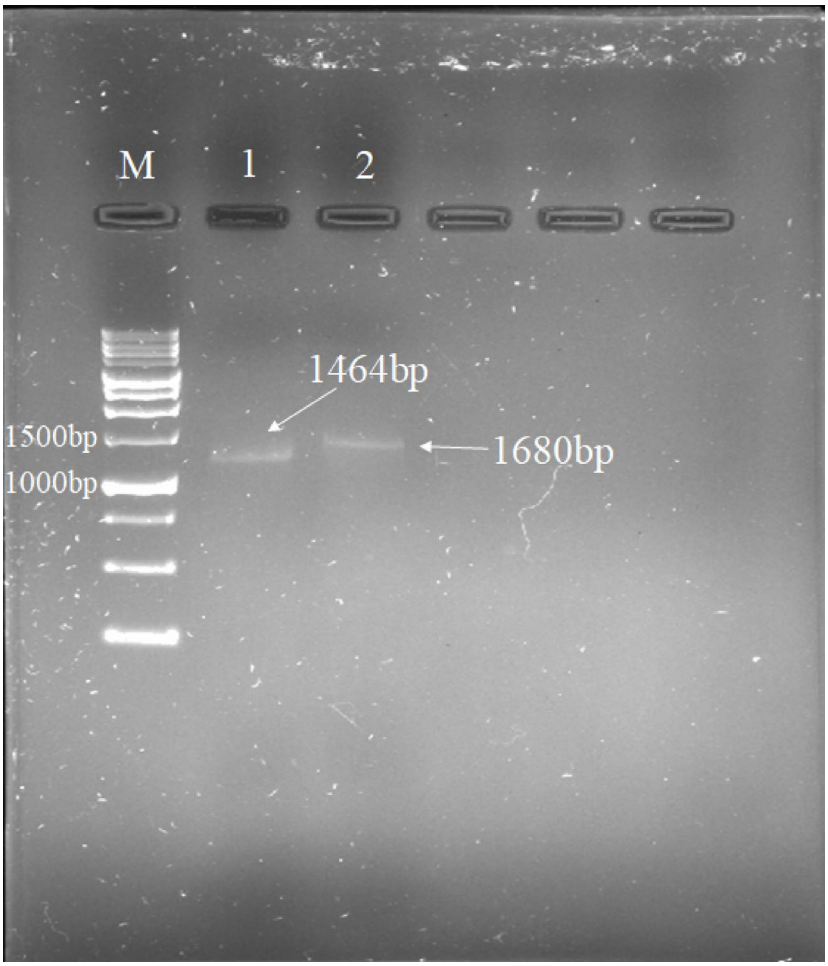

Fig. 1. Agarose gel electrophoresis of; lan 1, amplified purified PCR *ACPase* (1464 bp); lan 2, amplified purified PCR *ALPase* (1680 bp); M, 10.000 bp DNA ladder (Invitrogen, California, USA).

bp, respectively. In the anticipated duration of the *ACPase* and *ALPase* genes in *Streptomyces* sp. MMA-NRC, at the first time. These genes sequence encodes a protein comprising 488 and 560 amino acids, respectively. The comparison also showed that the *ACPase* and *ALPase* genes and translated proteins from *Streptomyces* sp. MMA-NRC shared 99% similarity with *ACPase* and *ALPase* genes of *Streptomyces* sp. 4 F, as descriped in Fig. 1, and showed 0.0 E-values, 2710 and 3103 alignment score for *ACPase* and *ALPase* genes of *Streptomyces* sp. MMA-NRC; respectively. Consequently, the obtained sequence for the *ACPase* and *ALPase* genes was submitted to the NCBI database with the accession numbers PV646716 and PV646717 for *Streptomyces* sp. MMA-NRC, respectively. Subsequently, Protein *ACPase* and *ALPase* was represented by their respective amino acid sequences, which were generated from the nucleotide sequences of the genes. We used the UniProt protein database to find three more *ACPase* and *ALPase* sequences that corresponded with the amino acid sequence. Additionally, the InterProScan server (EMBL) identified amino acid 1-488 and 1-560 residues as belonging to the *ACPase* and *ALPase* families.

In a related study of[41], performed a phylogenetic analysis using bacterial PP2C *phosphatase* sequences from the InterPro database, classifying the family into five groupings. investigated the evolutionary links, species distribution, sequence and structural changes, and domain distribution features of bacterial PP2C phosphatases based on this classification. Evidence of a shared evolutionary origin for bacterial PP2C phosphatases was found by our analysis. By providing important information for upcoming functional investigations of bacterial serine/threonine phosphatases and supporting the development of targeted treatments for harmful bacteria, these discoveries enhance our knowledge of PP2C phosphatases[42], reported the gene encoding *alkaline phosphatase* designated *phoK* was amplified and sequenced from of *Sphingomonas* sp. strain BSAR-1[43], using genomic DNA as a template, the gene encoding putative thermostable *Alkaline Phosphatase APase* was sequenced from *B. licheniformis* MTCC1483. According to sequence analysis, the gene was 1662 bp long (GenBank accession number KF577606) and was expected to code for a 553 amino acid polypeptide[44], reported the *olpA* gene of *Chryseobacterium meningosepticum*, encoding a molecular class C *phosphatase*, was amplified and sequenced[45], reported M2-32 is a non-specific *acid phosphatase* was amplified and sequenced, with a rare ability to function across a broad pH range (3.5–8.5). Analysis using SWISS-PROT Prf Profiles classifies it as a class A *acid phosphatase* (Z-score: 78.97), sharing 50%-60% sequence similarity with enzymes such as *PhoC* and *PhoN*[46], reported twelve

clinical isolates and two reference strains of *S. aureus* had their *SapS* gene extracted and sequenced; in silico PCR was used to test 49 *S. aureus* strains and 11 coagulase-negative staphylococci. Semi-purified protein extracts from the clinical strains' culture medium were tested for *phosphatase* activity using a variety of *phosphatase* inhibitors in combination with p-nitro-phenylphosphate, O-phospho-L-tyrosine, O-phospho-L-serine, and OphosphoL-threonine[47], reported genomic sequence analysis of *Acinetobacter baumannii* revealed the presence of a putative *Acid Phosphatase* (AcpA; EC 3.1.3.2)[48], initially, 21 amino acid sequences of the *alkaline phosphatase* enzyme from several *P. aeruginosa* strains were obtained. In BLAST, the amino acid sequences displayed a minimum similarity of 99% and a maximum similarity of 100%. *P. aeruginosa* PAO1, *P. aeruginosa* UCBPP-PA14, *P. aeruginosa* VRFPA05, *P. aeruginosa* PAO579, *P. aeruginosa* HB13, *P. aeruginosa* DHS01, *P. aeruginosa* CI27, *P. aeruginosa* MPAO1/P2, *P. aeruginosa* PADK2_CF510, *P. aeruginosa* CIG1, *P. aeruginosa* E2, *P. aeruginosa* PA45, *P. aeruginosa* VRFPA02, *P. aeruginosa* VRFPA03, *P. aeruginosa* VRFPA07, and *P. aeruginosa* VRFPA08.

Cluster analysis (phylogenetic tree) of Streptomyces sp. strain MMA-NRC ACPase and ALPase proteins

After sequence analysis, a phylogenetic investigation was performed to ascertain the position of the *ACPase* and *ALPase* proteins within the larger framework of known phosphatase family members. In this investigation, a carefully selected dataset of 10 *ACPase* and *ALPase* proteins from various species was chosen from the UniProt protein database. One of the proteins in question is *ACPase* and *ALPase* proteins derived from *Streptomyces* sp. strain MMA-NRC. A comparison revealed that the *ACPase* and *ALPase* protein of *Streptomyces* sp. MMA-NRC has a sequence similarity of 99% with the *ACPase* and *ALPase* proteins of *Streptomyces* sp. strain 4 F, which are also part of the *streptomyces* genus. The BLAST program was used to generate the phylogenetic tree, utilizing the *ACPase* and *ALPase* proteins sequences from the 10 *streptomyces* strains. The results revealed a *Streptomyces* sp. strain MMA-NRC and *Streptomyces* sp. strain 4 F were classified and closely associated with putative *ACPase* and *ALPase* proteins.Additional information on the phylogenetic connections among these strains is provided in Fig. 2.

In a related study of[41], reported 57,520 amino acid sequences were obtained from the PP2C family entry PF13672 at InterPro using phylogenetic analysis. Bacteria from nearly every taxonomic group provide the majority of these sequences. Bacterial PP2C phosphatases were shown to have a common ancestor in the resultant phylogenetic tree, indicating that these genes may have shared an ancestry and have maintained important biological activities across time. The phylogenetic tree also revealed that the PP2C family may be categorised into five groups, which are designated Group I, II, III, IV, and V. There are 801, 764, 612, 647, and 749 sequences in each of these groupings, respectively, suggesting a fairly even distribution throughout the categories[49], using a variety of bioinformatics methods, thirty-three sequences six from each of the three classes of bacterial *acid phosphatase* and seven from archaeal *phosphoesterases* were examined. Three classes of bacterial *acid phosphatases* and archaeal *phosphoesterases* were compared and contrasted using phylogenetic analysis, dot plot comparisons, and motif analysis. Using a bioinformatics method, we have tried to determine the evolutionary relationships between three groups of bacterial *acid phosphatase* and archaeal phosphoesterases. The following are the names of bacteria and archaea, accompanied by the accession numbers in parenthesis: Class A bacterial *acid phosphatase* is represented by the digits 1 through 10. Class B *acid phosphatase* is represented by numbers 11–17, Class C *acid phosphatase* by numbers 18–26, and *Archaeal phosphoesterase* by numbers 27–33[13], reported class C genes are more widely distributed; their association with the outer-membrane of cells gives them a clear role in the cycling of organic phosphorus, especially in soils. Bacterial Non-Specific *Acid Phosphatase* (*NSAP*) enzymes were used to determine *NSAP* diversity and subcellular localization in microbial genomes; corresponding *NSAP* gene sequences were used to census metagenomes from diverse ecosystems; and researchers examined the impact of long-term land management on *NSAP* diversity and abundance[41], study the structural similarities and differences among PP2C phosphatases in the five identified groups, five PP2C *phosphatases* Q8VQA1 (PDB ID: 2PK0), P9WHW5 (PDB ID: 1TXO), A0A1L7GEB2, A0A7V6HC85, and P76395 corresponding to five groups of Group I, II, III, IV, and V, separately, were selected as representative proteins for detailed structural characterization[48]. A branching diagram called a phylogenetic tree aids in understanding the evolutionary relationships between biological species. Here, the phylogenetic tree was constructed using the MEGA6 software. Two phylogenetic trees were created in total. One phylogenetic tree comprising the *alkaline phosphatase* amino acid sequences from various *P. aeruginosa* strains. Another one made up the cDNA of the protein found in various *P. aeruginosa* strains. In the phylogenetic tree of the amino acid sequences of *alkaline phosphatase* of selected strains of *P. aeruginosa* showed mainly three major groups present.

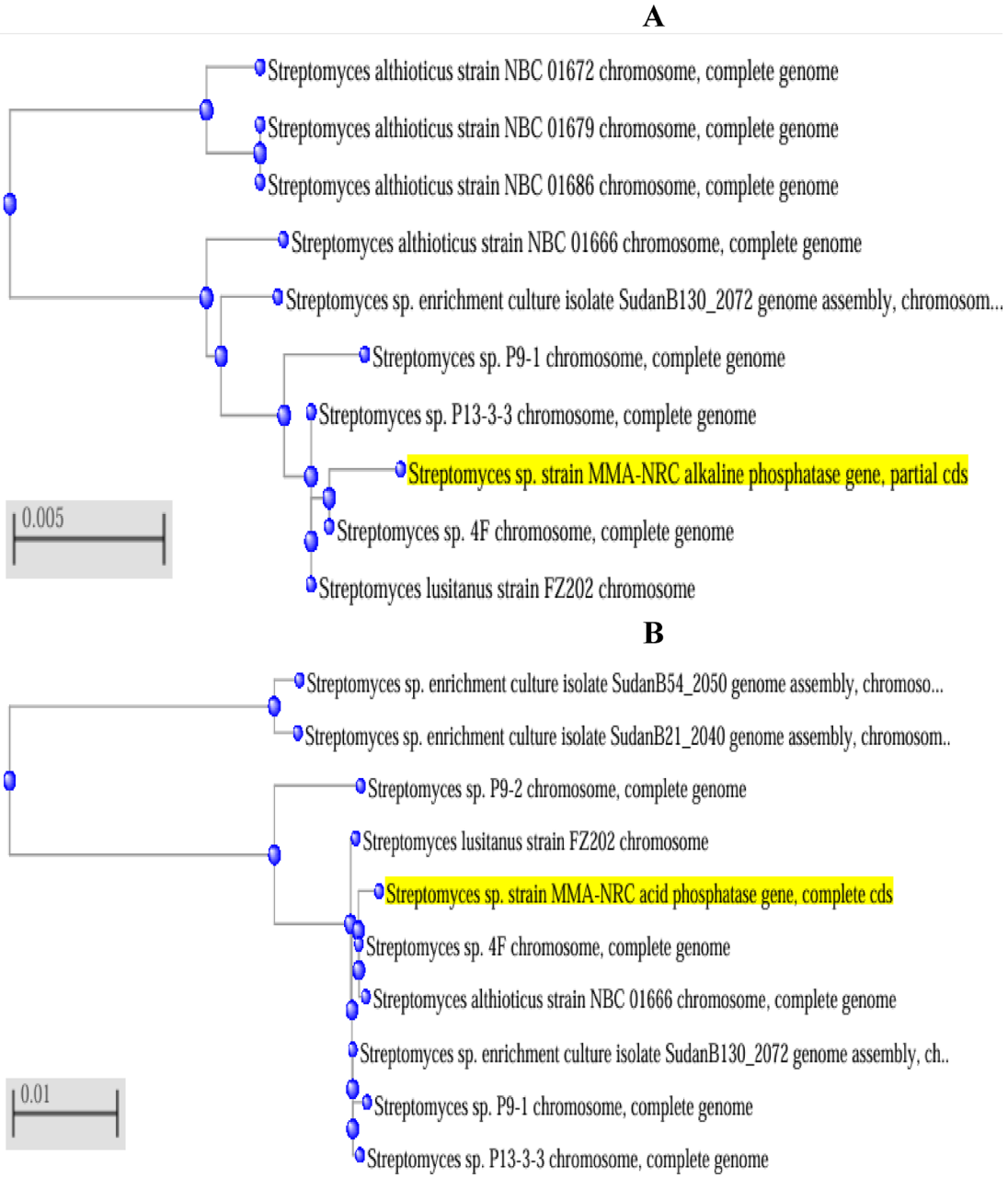

Fig. 2. Phylogenetic tree of ten *Streptomyces* strains and *Streptomyces* MMA-NRC **(a)***ALPase* and **(b)***ACPase* protein sequences and other *phosphatase* proteins, constructed using the neighbor-joining method (BLAST) software.

Secondary structure prediction of ACPase and ALPase protein

Use the template *Streptomyces sp.*4F and wild type *Streptomyces sp MMA-NRC* to align the *ACPase* 488 residues and *ALPase* 500 residues (from 560 residues) proteins and predict their secondary structures. The experiments were conducted using the PDBsum service.

According to the *ACPase* model characterization in the PDBsum, the predicted *ACPase* enzyme for template *Streptomyces sp.*4F has the following secondary structure: has 23 helix and 35beta turn, as shown in Fig. 3a. In contrast, wild type *Streptomyces sp MMA-NRC* has 24 α-helices and 23 β-turn, as shown in Fig. 3b.

According to the *ALPase* model characterization in the PDBsum, the *ALPase* enzyme in template *Streptomyces sp.*4F is expected to have the following secondary structure: has 15 helix and 51 beta turn, as shown in Fig. 3c. In contrast, wild type *Streptomyces sp MMA-NRC* has 13 α-helices and 47 β-turn, as shown in Fig. 3d.

Reference[41], study the structural similarities and differences among PP2C *phosphatases* in the five identified groups. As depicted in result of structure superposition, a core β sandwich made up of anti-parallel β slices and two anti-parallel helices on either side of the β slices in an alpha-β-β-α configuration were among the secondary structural units that the bacterial PP2C *phosphatases* had in common. However, the five groups' secondary

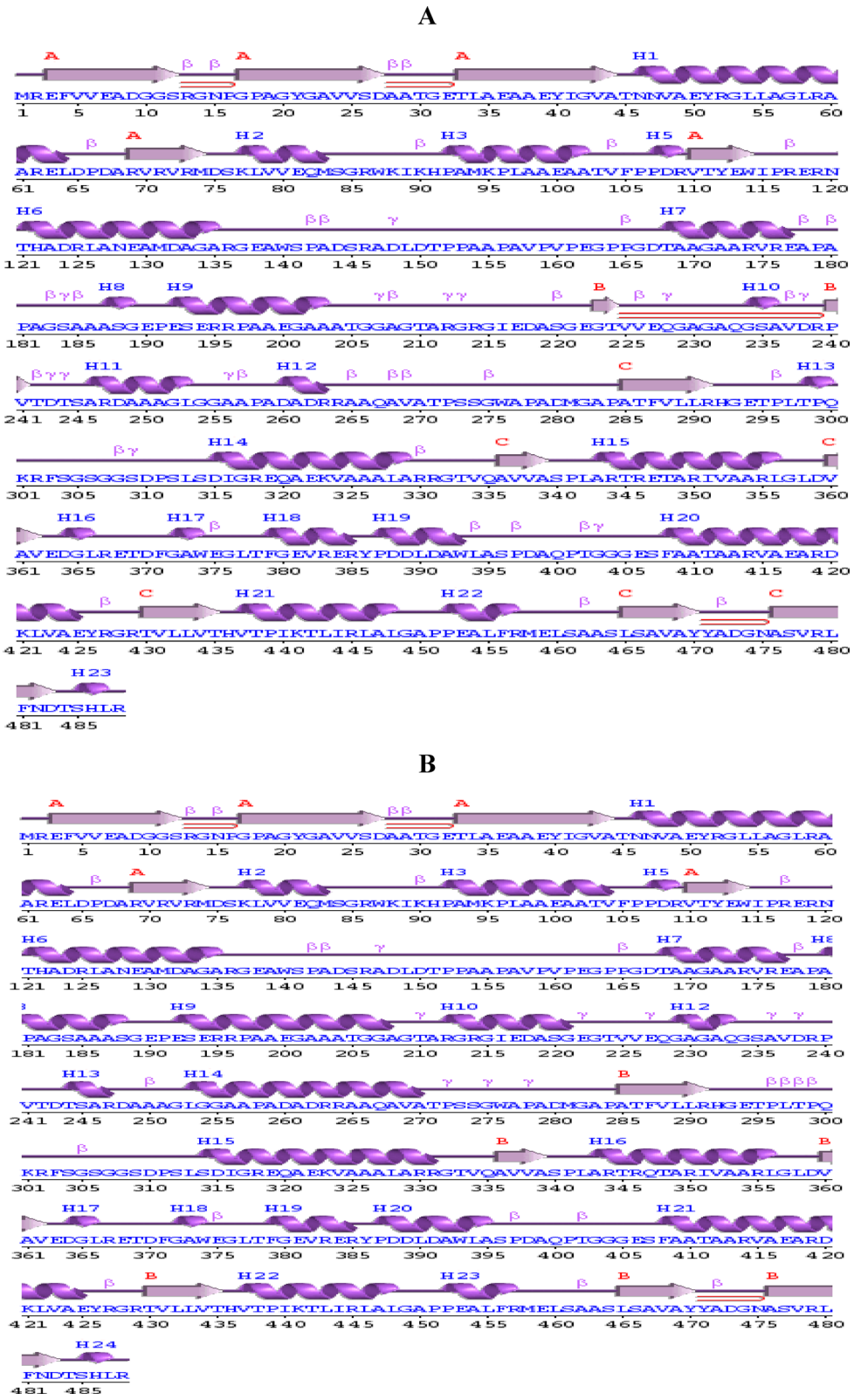

Fig. 3. Predicted *ACPase* and *ALPase* proteins secondary structure of **(A)** template *Streptomyces sp.4 F ACPase*; **(B)** wild type *Streptomyces sp MMA-NRC ACPase*; **(C)** template *Streptomyces sp.4 F ALPase*; **(D)** wild type *Streptomyces sp MMA-NRC ALPase.*

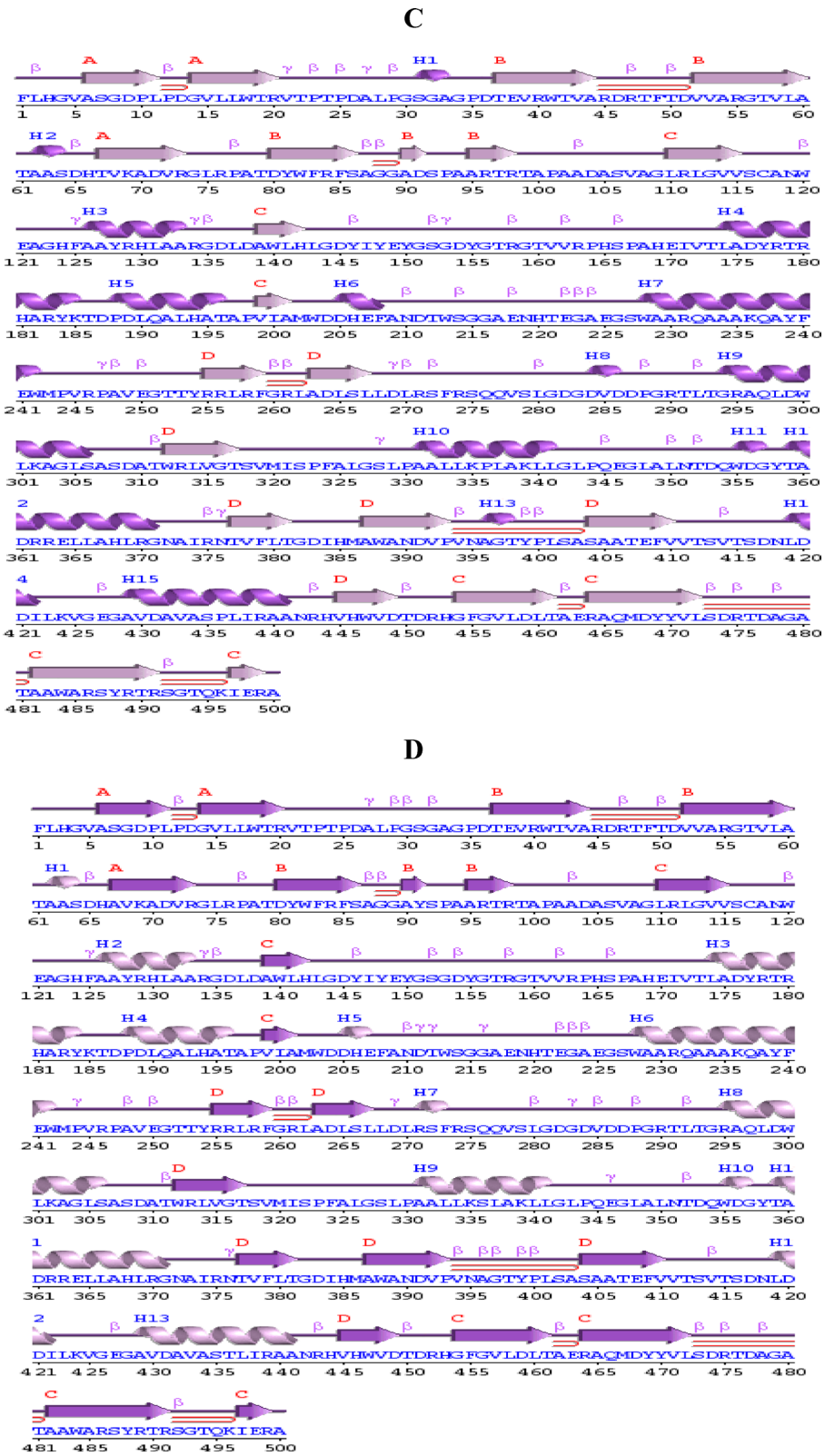

Fig. 3. (continued)

structural components also exhibit variations. In the core β-sandwich, there were varying numbers of β-strands: Groups I and II had ten β-strands, Groups III and V had nine, and Group IV had eleven. These variations could be the cause of these *phosphatases*' functional peculiarities. The flap subdomain in PP2C phosphatases is a characteristic of proteins belonging to Groups I, II, and III that includes frontal extension α-helices in addition

to the pair of antiparallel helices flanking the β-sheet[45]. , determined the x-ray crystal structure of non-specific *acid phosphatase* M2-32 by molecular replacement using an AlphaFold2-guided truncated model, achieving a resolution of 2.2 Å. The protein crystallized as a dimer-of-dimers. Each monomer (residues 38–274) adopts an all-alpha-helical fold composed of 14 helices and two disulfide bonds[48], *alkaline phosphatase* were predicted by PSI-blast based secondary structure PREDiction (PSIPRED) and Chou and Fasman secondary structure prediction (CFSSP) server (http://cho-fas.sourceforge.net/index.php). The findings of the secondary structure prediction showed that the percentage of alpha helices was significantly higher than the percentage of other protein conformations, such as sheet and turn. Most of The strains of *P. aeruginosa* displayed the 63.7% helix. However, EME95396 and ERF08779.1 were the exceptions.Alpha helices were present in 64.7% of *P. aeruginosa* HB13 and *P. aeruginosa* PA21_ST175 samples. The percentage of betasheet was 54%, the same for all selected strains of P. aeruginosa.Additionally, the proportion of turn was nearly the same across all *P. aeruginosa* strains. The only one with a 14.5% turn was ETD45171.1 (*P. aeruginosa*VRFPA07). A detailed determination of the secondary structure of the amino acid sequence of P. aeruginosa PAO1's alkaline phosphatase was made. There were no abnormal protein binding sites found.

Homology modeling and validation of ACPase and ALPase proteins

Using Robetta server, five models were generated for the *acid phosphatase* (*ACPase)* 488 residues and alkaline *phosphatase* (*ALPase)* 500 residues from 560 residues (Robetta server do not accept more than 500 amino acids for protein modeling), for both the template *Streptomyces sp.*4F and wild type *Streptomyces sp MMA-NRC;* respectively.

Determined by the density of their clusters. The confidence ratings (C-scores) for the five various models of the *ACPase* residues. Model 5, with the highest C-score and low estimation error, the sample was chosen for additional examination because to its high C-score, which indicates a strong level of confidence in the model was 0.73 for template strain *Streptomyces sp.*4F, as illustrated in Fig. 4a. Model 1, with the highest C-score and low

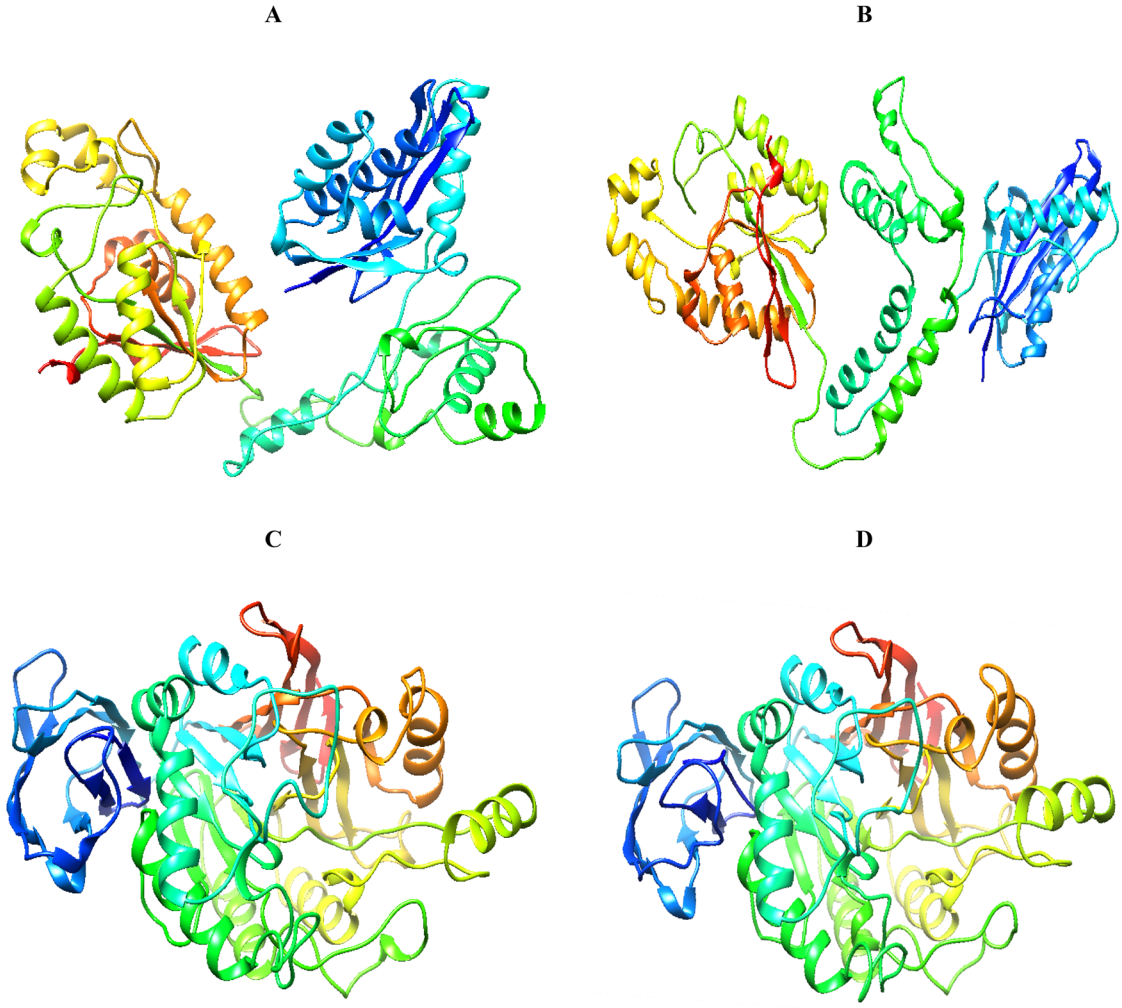

Fig. 4. Modelled 3D structure of *ACPase* and *ALPase proteins*: **(A)** template *Streptomyces sp.4 F ACPase*; **(B)** wild type *Streptomyces sp MMA-NRC ACPase*; **(C)** template *Streptomyces sp.4 F ALPase*; **(D)** wild type *Streptomyces sp MMA-NRC ALPase.*

estimation error, the data was chosen for additional examination because to its high C-score, which indicates a strong level of confidence in the model was 0.72 for wild type strain *Streptomyces sp MMA-NRC*, as illustrated in Fig. 4b.

Determined by the density of their clusters. The confidence ratings (C-scores) for the five various models of the *ALPase* residues. Model 1, with the highest C-score and low estimation error, the sample was chosen for additional examination because to its high C-score, which indicates a strong level of confidence in the model was 0.86 for template strain *Streptomyces sp.*4F as illustrated in Fig. 4c. Model 1, with the highest C-score and low estimation error, the sample was chosen for additional examination because to its high C-score, which indicates a strong level of confidence in the model was 0.85 for wild type strain *Streptomyces sp MMA-NRC* as illustrated in Fig. 4d.

Subsequently, the model that was produced underwent evaluation using general stereo chemical parameters using the PROCHECK website. In addition, the *Ramachandran* plot was developed for the energy-minimized model of *ACPase* and *ALPase* structures for *Streptomyces sp.*4F and *Streptomyces sp.*MMA-NRC. The x-axis of the plot is divided into four quadrants, which correspond to the low-energy area, permitted region, usually allowed region, and prohibited region, as shown in Table 1.

The 3D modeled for template strain *Streptomyces sp.*4F *ACPase* protein underwent analysis using PROCHECK, which indicated that 488 residues, accounting for 100% overall quality factor, representing 91.04% of the total quality factor, were 92.2% located in the most favorable areas of the Ramachandran plot. In addition, 7.5% of residues were found in the further permitted areas, 0.2% in the generously allowed regions, and lowest 0.0% in the disallowed regions, which indicate model stability, as illustrated in Fig. 5a.

The 3D modeled strain for wild type strain *Streptomyces sp MMA-NRC ACPase* protein was analyzed using PROCHECK, which revealed that 488 residues, accounting for 94.37% overall quality factor (94.5% The majority of residues were located inside the most favorable sections of the Ramachandran plot. In addition, 4.8% of the residues were found in the extra permitted areas, 0.8% in the generously allowed regions, and lowest 0.0% in the disallowed regions, which indicate model stability, as illustrated in Fig. 5b.

The 3D modeled for template strain *Streptomyces sp.*4F *ALPase* protein was analyzed using PROCHECK, which revealed that 500 residues, accounting for 92.16% overall quality factor (86.8% The majority of residues were located inside the most preferred areas of the Ramachandran plot. In addition, 11.8% of the residues were located in the extra permitted zones, 1.2% in the generously allowed regions, and lowest 0.2% in the disallowed regions, which indicate model stability), as illustrated in Fig. 5c.

The 3D modeled wild type strain *Streptomyces sp MMA-NRC ALPase* protein was analyzed using PROCHECK, which revealed that 500 residues, accounting for 93.08% overall quality factor (87.8% The majority of residues were located inside the most preferred areas of the Ramachandran plot. In addition, 10.4% of the residues were located in the extra permitted zones, 0.9% in the generously allowed regions, and 0.9% in the disallowed regions, which indicate model stability), as illustrated in Fig. 5d.

In related studies of[41], the UniProt database was used to retrieve representative protein structures from five phylogenetic groups: P9WHW5 (PDB ID: 1TXO) from *M. tuberculosis*, A0A1L7GEB2 (AlphaFold ID: AF-A0A1L7GEB2-F1) from *Streptomyces sp*. TN58, A0A7V6HC85 (AlphaFold ID: AF-A0A7V6HC85-F1) from the *Clostridiaceae* bacterium, Q8VQA1 (PDB ID: 2PK0) from *S. agalactiae*, and P76395 (AlphaFold ID: AF-P76395-F1) from *Escherichia coli*. The other three proteins were predicted structures derived from AlphaFold, with the exception of the PP2C from *S. agalactiae* (PDB ID: 2PK0) and *M. tuberculosis* (PDB ID: 1TXO), which represented the known structure in bacteria. The amino acid residues from the active centre were then labelled based on the sequence alignment results after the five typical protein structures were superimposed using ChimeraX software. Lastly, the primary to quaternary protein structure data of five sample proteins were examined using ESPript[50]. , the native enzyme structures were superimposed with their corresponding AlphaFold2-predicted QTY variants, demonstrating a high degree of structural similarity. These findings support the effectiveness of the QTY code for modeling β-barrel membrane enzymes and highlight its potential utility in designing water-soluble membrane proteins for a broad range of biological applications[51]. , using a combination of forward genetics, biochemical reconstitution, and AlphaFold2 structure prediction, identified a conserved, tripartite substrate docking interface comprised of three variable loops on the surface of the PPM *phosphatase* domains of *SpoIIE* and *RsbU* that recognize the 3D three-dimensional structure of the substrate protein[43]. , comparison modeling of the recombinant of *BlAPase* amino acid sequence with that of a few other bacterial *alkaline phosphatases*. Their active site areas involved in phosphate binding, phosphorylation, and metal binding are substantially conserved, according to the multiple alignment study. The recombinant *BlAPase* showed the highest level of similarity with *B. licheniformis* MC14 *APase*. Compared to *Bacillus subtilis*, *C. marina*, *E. coli*, *antarctic* strain Table 5, *T. thermophilus* HB27, and *Meiothermus ruber*, the enzyme's amino acid sequence showed 37, 32, 31, 31, 28, and 27% similarity, respectively. In recombinant *BlAPase*, the amino acid residues

	Overall quality factor %	Most favored rejoin%	Additional allowed rejoin%	Generously allowed rejoin%	Disallowed rejoin %
*Streptomyces sp.*4f-*ACPase*	91.04	92.2	7.5	0.2	0.0
Streptomyces sp.-MMA-NRC *ACPase*	94.37	94.5	4.8	0.8	0.0
*Streptomyces sp.*4f-*ALPase*	92.16	86.8	11.8	1.2	0.2
Streptomyces sp.- MMA-NRC *ALPase*	93.08	87.8	10.4	0.9	0.9

Table 1. Ramachandran plot energy-minimized model of *ACPase and alpase* of *Streptomyces sp.*4f and *Streptomyces sp.*-MMA-NRC.

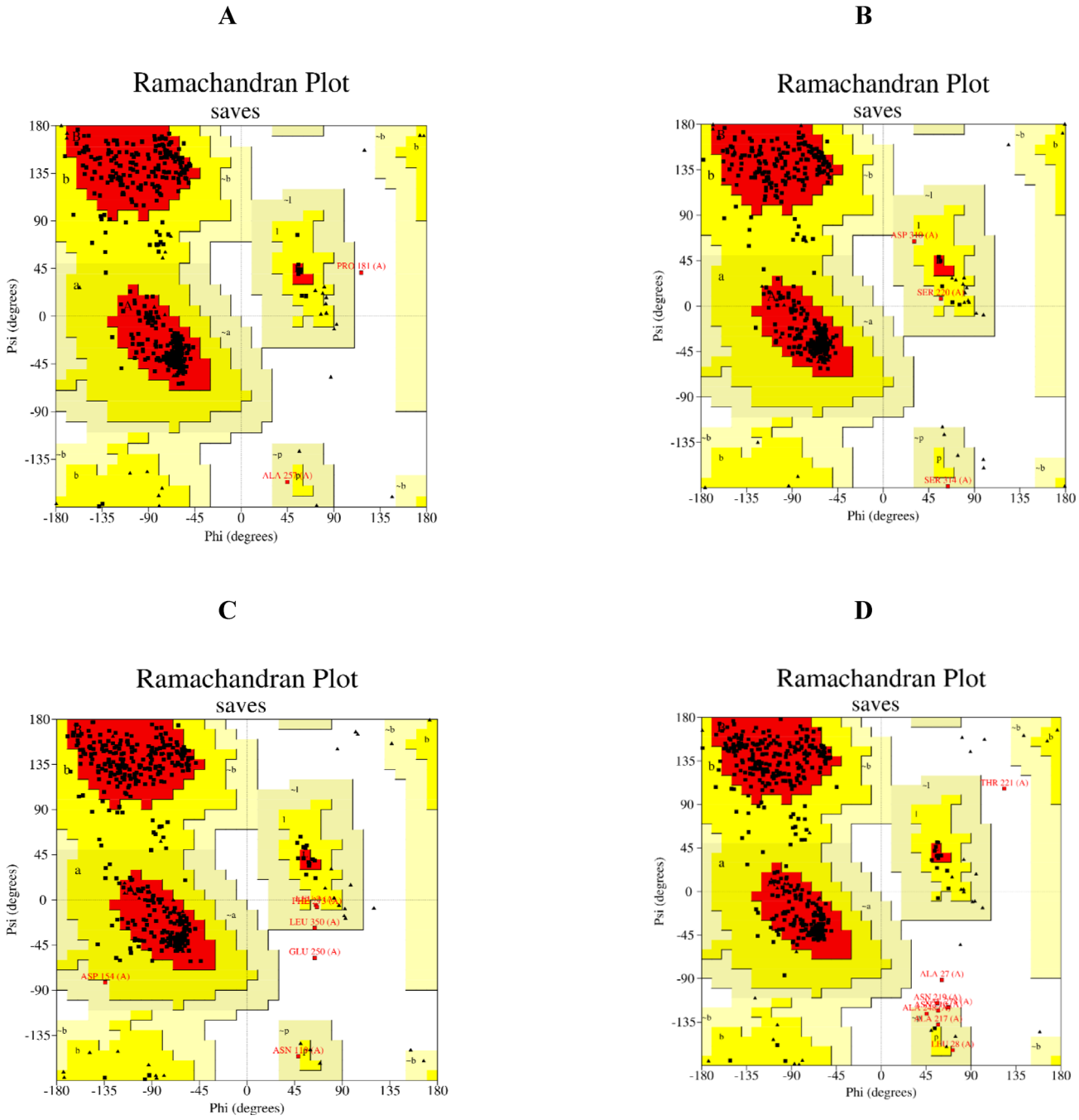

Fig. 5. Ramachandran plot of *ACPase* and *ALPase proteins*: **(A)** template *Streptomyces sp.4 F ACPase*; **(B)** wild type *Streptomyces sp MMA-NRC ACPase*; **(C)** template *Streptomyces sp.4 F ALPase*; **(D)** wild type *Streptomyces sp MMA-NRC ALPase.*

Asp49, Ser89, Thr150, Arg168, Glu283, Asp288, His292, and Asp307 are highly conserved[48]. , the comparative homology protein model of *P. aeruginosa* PAO1 *alkaline phosphatase* was predicted using the SWISS-Model Workspace. In this case, 1alh.1. A, the crystal structure of a mutant *E. coli alkaline phosphatase*, was chosen as the template sequence. 73.93% of the template sequence and the query sequence were identical. The structure's resolution was 2.50␣ The projected protein model's oligo state was homo dimer. The *alkaline phosphatase* of *P. aeruginosa* PAO1 predicted protein model was assessed and confirmed using the QMEAN and SAVES servers. From SAVES, ERRAT, Ramachandran plot, and 3D verification were assessed. The Ramachandran plot analysis showed that 97.0% of the residues were in the favored (red) region, 4.7% were in the allowed (brown) regions, and the remaining 2.6% were in the generously allowed (yellow) or outlier region. A high-quality model has more than 90% of its residues in the favored region.

Docking and molecular interaction studies

Using the HDock online tool, docking studies were carried out to investigate how the substrate rock phosphate binds to the 3D model of the *ACPase* and *ALPase* protein. For the docking procedure, the receptor and ligand files were saved in pdb format. The nonpolar hydrogen atoms were mixed with the carbon atoms, and the polar H atoms were given Gasteiger charges. The required adjustments were made to the internal degrees of freedom and torsions. Low distance and strong inertaction between the ligand and protein receptor were suggested by active site amino acids with the lowest degree of interface residues.

The docking results of rock phosphate with the 3D model of *ACPase* showed the patterns of interaction. With an affinity score of -116.76 kcal/mol, a confidence score of 0.3397, a ligand RSMD (Å) of 34.22, and active site amino acids of ARG291 and PHE456 with low interface residues of 2.345 and 2.103, respectively, the template strain *Streptomyces sp*. 4f *ACPase*.

The docking results of rock phosphate with the 3D model of *ACPase* showed the patterns of interaction. The wild type strain *Streptomyces sp*. MMA-NRC *ACPase* had an affinity score of -110.86 kcal/mol, a confidence score of 0.3137, a ligand RSMD (Å) of 69.31, and active site amino acids ARG91 and THR298 with low interface residues of 2.105 and 2.262, respectively, as shown in Table 2. Demonstrated aromatic interaction, H-Bond interaction, and hydrophobic interaction, as shown in Fig. 6.

The docking results of rock phosphate with the 3D model of *ALPase* showed the patterns of interaction. For the template strain *Streptomyces sp*. 4f *ALPase* strain, the affinity score of -129.64 kcal/mol, confidence score of 0.3996, ligand RSMD (Å) of 29.86, and active site amino acids of HIS385 and ASP417 with low interface residues of 2.135 and 2.033, respectively,

The docking results of rock phosphate with the 3D model of *ALPase* showed the patterns of interaction. For the wild type *Streptomyces sp.* strain MMA-NRC *ALPase*, the affinity score of -108.55 kcal/mol, confidence score of 0.3039, ligand RSMD (Å) of 33.68, and active site amino acids of GLN354 and HIS385 with low interface residues of 2.146 and 1.465, respectively, as shown in Table 2. Demonstrated aromatic interaction, H-Bond interaction, and hydrophobic interaction, as shown in Fig. 7.

In another investigation conducted by[41], found that conserved Asp and Gly residues were primarily grouped at the active core locations within motifs 1, 2, 5, 8, and 11 when we looked at the superposition diagram with labelled conserved amino acids. In line with the active center of eukaryotic PP2C *phosphatase*, conserved Asp residues found in motifs 2, 8, and 11 joined forces with two manganese ions to form a binuclear metal centre. Notably, examination of the PDB structures of the representative proteins from Groups I and II revealed that the active center of bacterial PP2C *phosphatase* contained a third metal ion. When the active centers of five protein groups were superimposed, it was revealed that conserved *Ser* residues in Group IV and conserved Asp residues in Motif 5 helped Groups I, II, III, and V bind the third metal ion. Furthermore, a comparison of the flap

ACPase		AlPase	
Active site amino acids	**Receptor interface residue(s)**	**Active site amino acids**	**Receptor interface residue(s)**
ARG 291	2.105	CYS 117	2.355
HIS 292	2.591	ASP 145	2.456
GLU 294	2.722	TYR 148	2.332
LEU 297	4.750	TYR 150	3.755
THR 298	2.262	TYR 155	3.493
PRO 299	3.274	ASP 204	4.870
LYS 301	4.754	HIS 206	2.688
ARG 302	4.009	ASP 211	3.379
PHE 303	3.700	GLN 277	4.024
SER 304	3.443	SER 279	4.901
LEU 342	4.289	LEU 280	3.325
ARG 344	3.026	SER 318	3.164
THR 345	4.609	VAL 319	3.271
PHE 371	2.692	MET 320	3.394
PHE 379	4.119	ASN 351	3.447
TRP 393	4.166	THR 352	4.100
LEU 394	4.123	ASP 353	2.366
PHE 408	4.381	GLN 354	2.146
THR 435	4.853	GLY 382	2.247
HIS 436	2.555	ASP 383	2.416
VAL 437	3.469	ILE 384	3.090
THR 438	2.872	HIS 385	1.465
ALA 462	4.974	SER 416	4.505

Table 2. Active site amino acids and receptor interface residue(s) of Docking interaction of *ACPase* and *ALPase* of wild type strain *Streptomyces* sp. MMA-NRC with rock phosphate substrate.

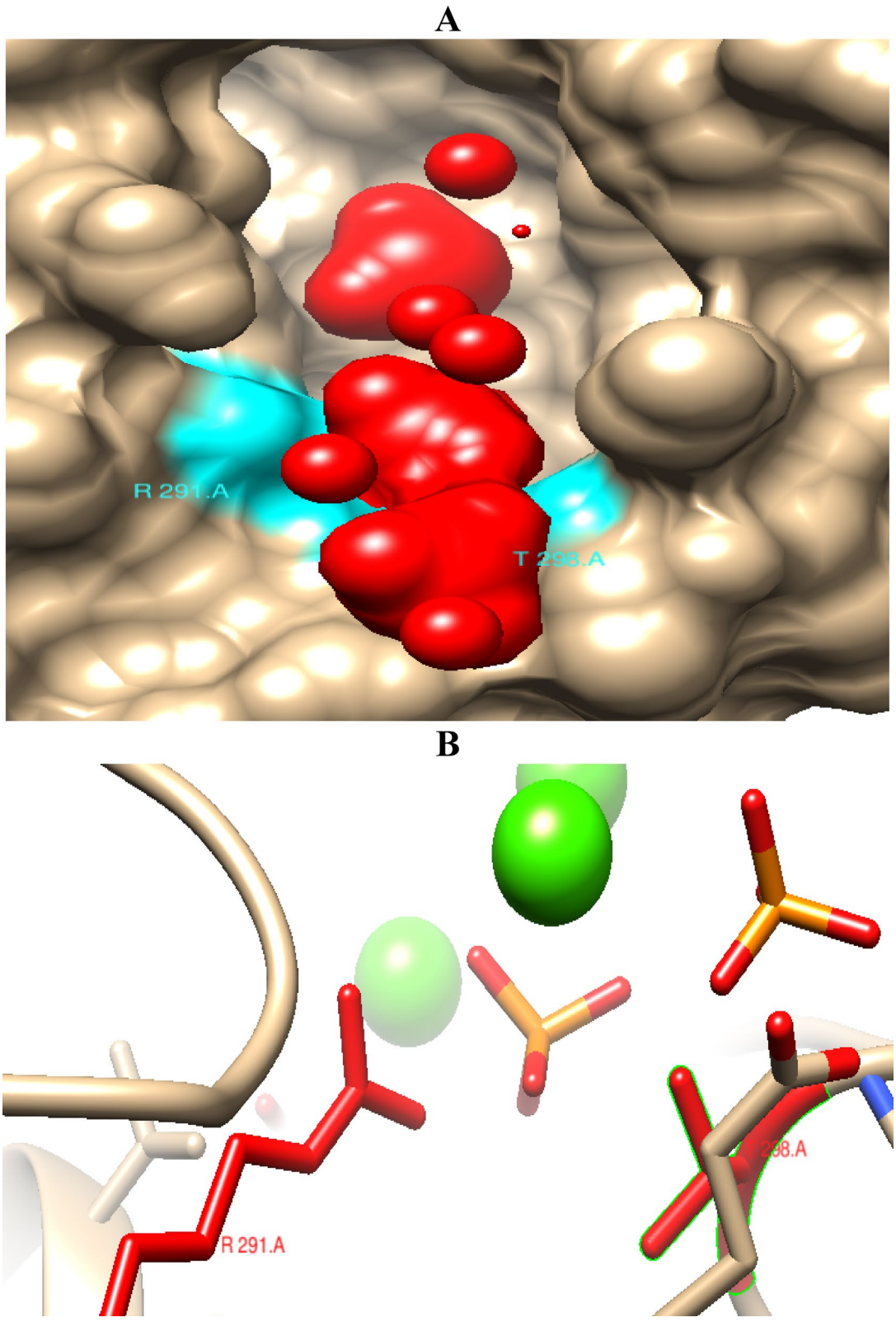

Fig. 6. protein–ligand docking by HDock of *Streptomyces sp.MMA-NRC ACPase*. **(A)** 3D surface. **(B)** 3D cartoon complex interaction showing binding *ACPase* with ligand rock phosphate displaying (red color) the most effective binding mode in the protein cavity (active site displayed by cyan color). **C;** Aromatic interaction, **(D)** H-Bond interaction and **(E)** Hydrophobic interaction.

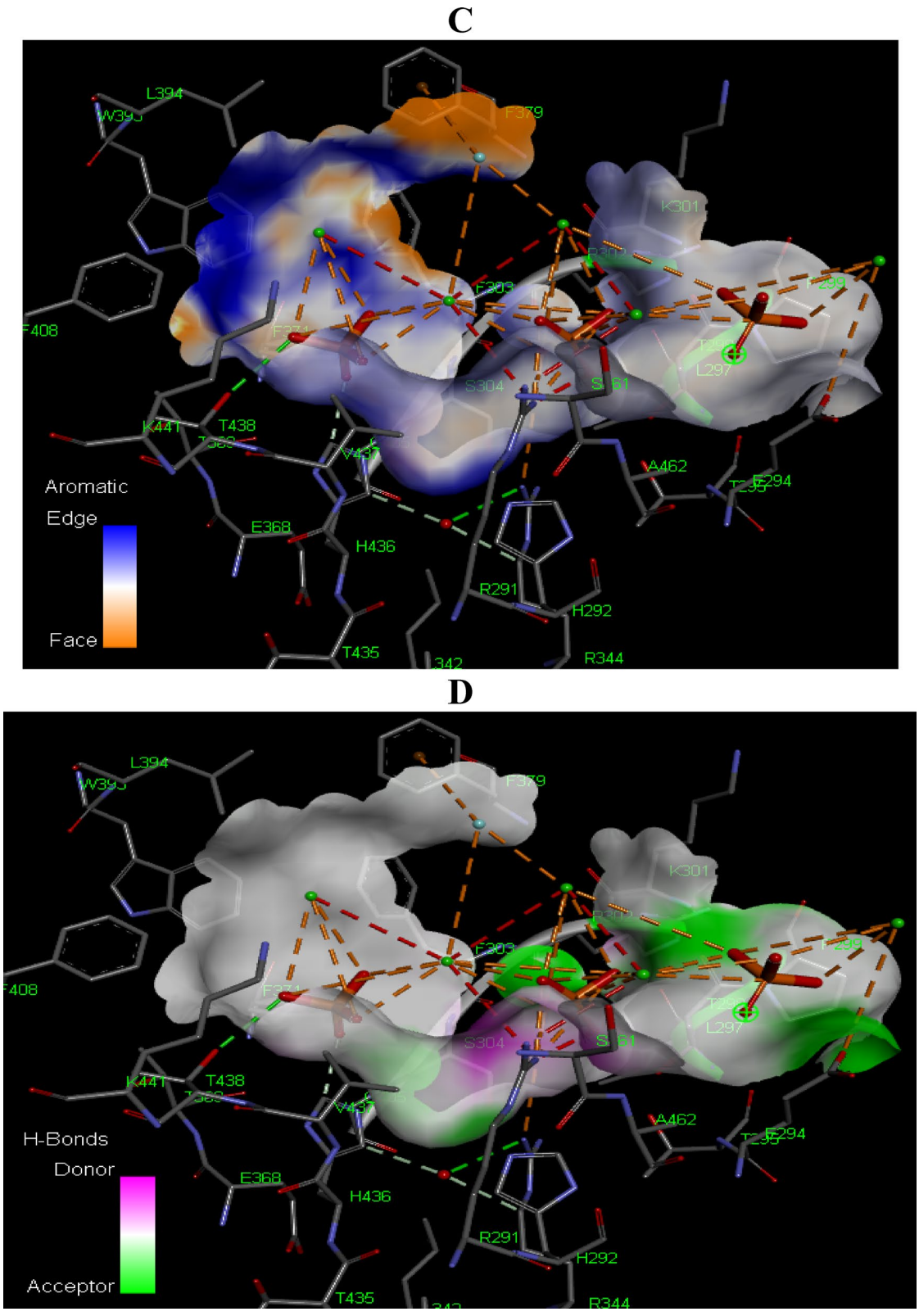

Fig. 6. (continued)

subdomains of the five typical proteins showed that Groups I, II, and III shared a lot in common, while Groups IV and V proteins showed a lot of variances. According to recent research, the flap subdomain was essential for the third metal ion's binding. We therefore speculate that the third metal ion would be common in the PP2C *phosphatases* of Groups I, II, and III based on these data. Additionally[45], , determined of non-specific *acid*

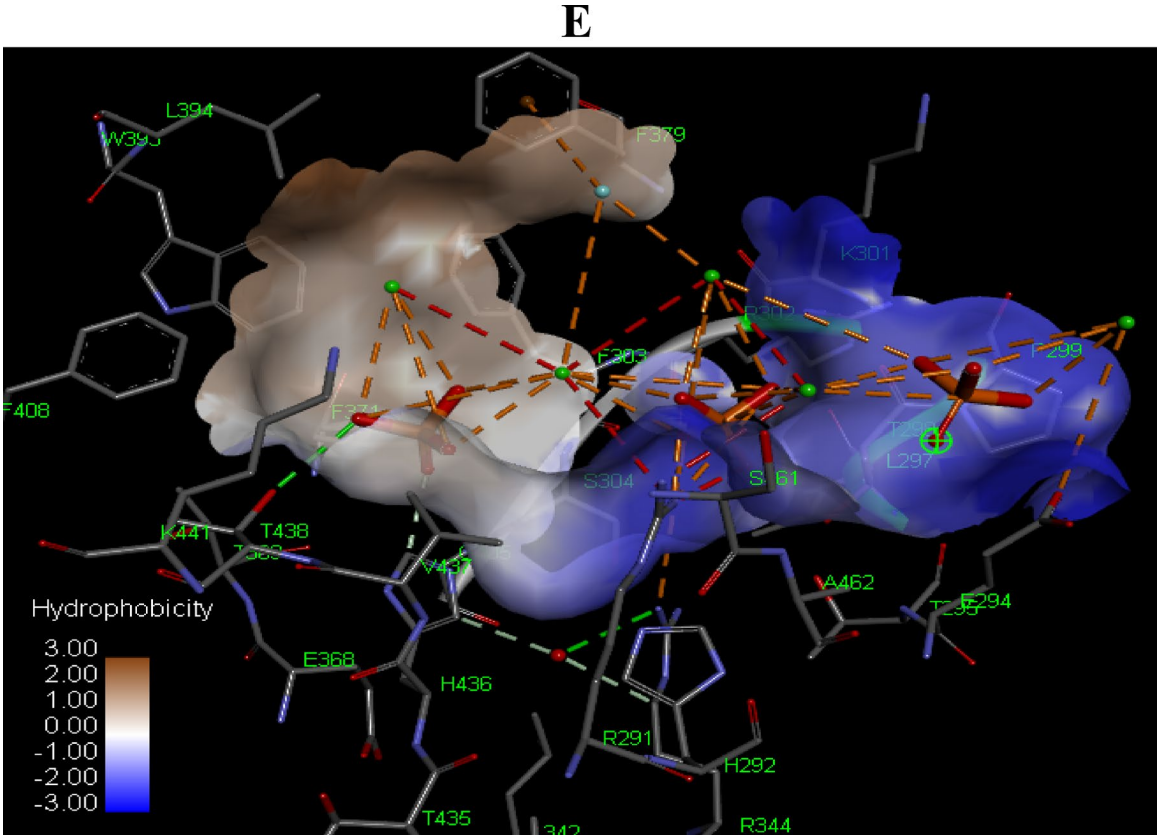

Fig. 6. (continued)

phosphatase M2-32 docking studies with adenosine monophosphates, combined with site-directed mutagenesis, identified His174, Arg207, His213, Asp217 as critical catalytic residues, and Tyr136 and Ser172 probably involved in substrate recognition. Mutations at these positions resulted in over 90% loss of enzymatic activity, highlighting their functional significance[51]. , reported the PPM *phosphatase* domains of *SpoIIE* and *RsbU*, nonconserved amino acids in these loops facilitate the accommodation of the cognate substrate and prevent dephosphorylation of the noncognate substrate. Together, single amino acid substitutions in these three elements cause an over 500-fold change in specificity. Data additionally suggest that substrate-docking interactions regulate phosphatase specificity through a conserved allosteric switch element that controls the catalytic efficiency of the *phosphatase* by positioning the metal cofactor and substrate. A generalizable mechanistic model for PPM family phosphatase substrate specificity.Importantly, the substrate docking interface with the phosphatase is only partially over lapping with the much more extensive interface with the upstream kinase, suggesting the possibility that kinase and phosphatase specificity evolved independently.

Cloning of *ACPase* and *ALPase* encoding genes in *E. coli DH5α*

The *ACPase* and *ALPase* encoding gene that scientists are studying is 1464 and 1680 bp long and comes from the *Streptomyces sp.* MMA-NRC. It is improved by using primers that are specific to the gene of interest. An analysis of the PCR results was performed using gel electrophoresis, which revealed the presence of two products measuring 1464 and 1680 bases in length, respectively, derived from genomic DNA. From what we can tell, the optimal circumstances for amplifying the target DNA amplicon were achieved at an annealing temperature of 57.5 °C. The Qiagen gel purification kit was used to remove the DNA band of the *Streptomyces sp.* MMA-NRC from the agarose gel. After that, a ligation cloning kit was used to clone it into the pGEM®-T Easy Vector. The cloning was done under T7 and SP6 strong promoters to enable the expression of *ACPase* and *ALPase*. The recombinant plasmid obtained was designated as *pGEM-T-ACPase* and *pGEM-T-ALPase*. The recombinant plasmid was introduced into the host organism for protein synthesis, *E. coli DH5α*, using the heat-shock method. The next step was to find transformants that could withstand ampicillin by using the white/blue screening approach, which included IPTG and X-gal. Different transformants derived from the *E. coli* strain were successfully produced by efficient transformation. The plasmids were extracted from *E. coli* transformants that were chosen at random and then subjected to analysis using agarose gel electrophoresis. PCR amplification was used to screen *E. coli* transformants containing genes for *ACPase* and *ALPase*. Specific primers utilized for the isolation of *ACPase* and *ALPase*, were employed for this purpose.

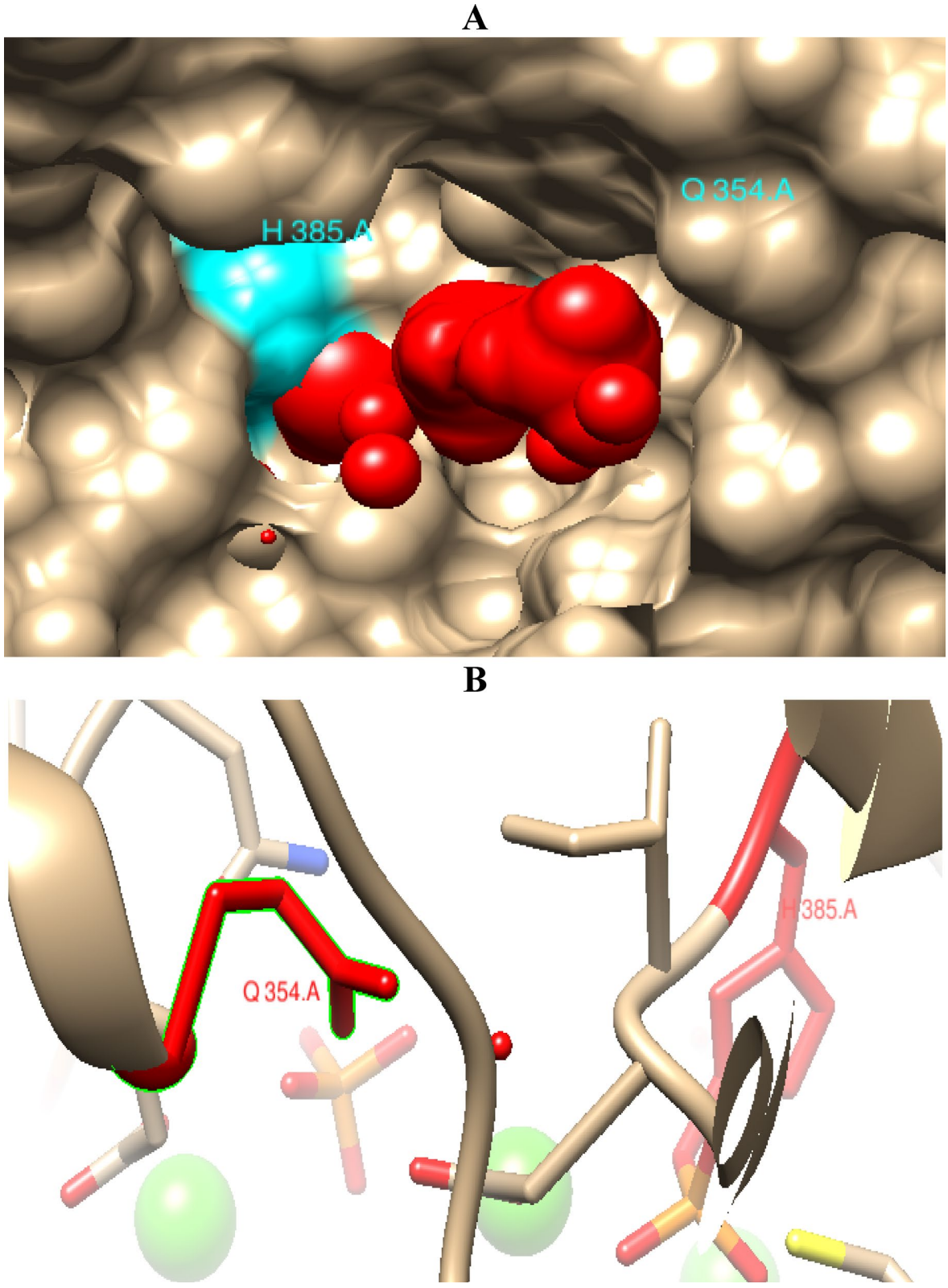

Fig. 7. protein–ligand docking by HDock of *Streptomyces sp.MMA-NRC ALPase*. **A;** 3D surface. **B;** 3D cartoon complex interaction showing binding *ALPase* with ligand rock phosphate displaying (red color) the most effective binding mode in the protein cavity (active site displayed by cyan color). **C;** Aromatic interaction, **D;** H-Bond interaction and **E;** Hydrophobic interaction.

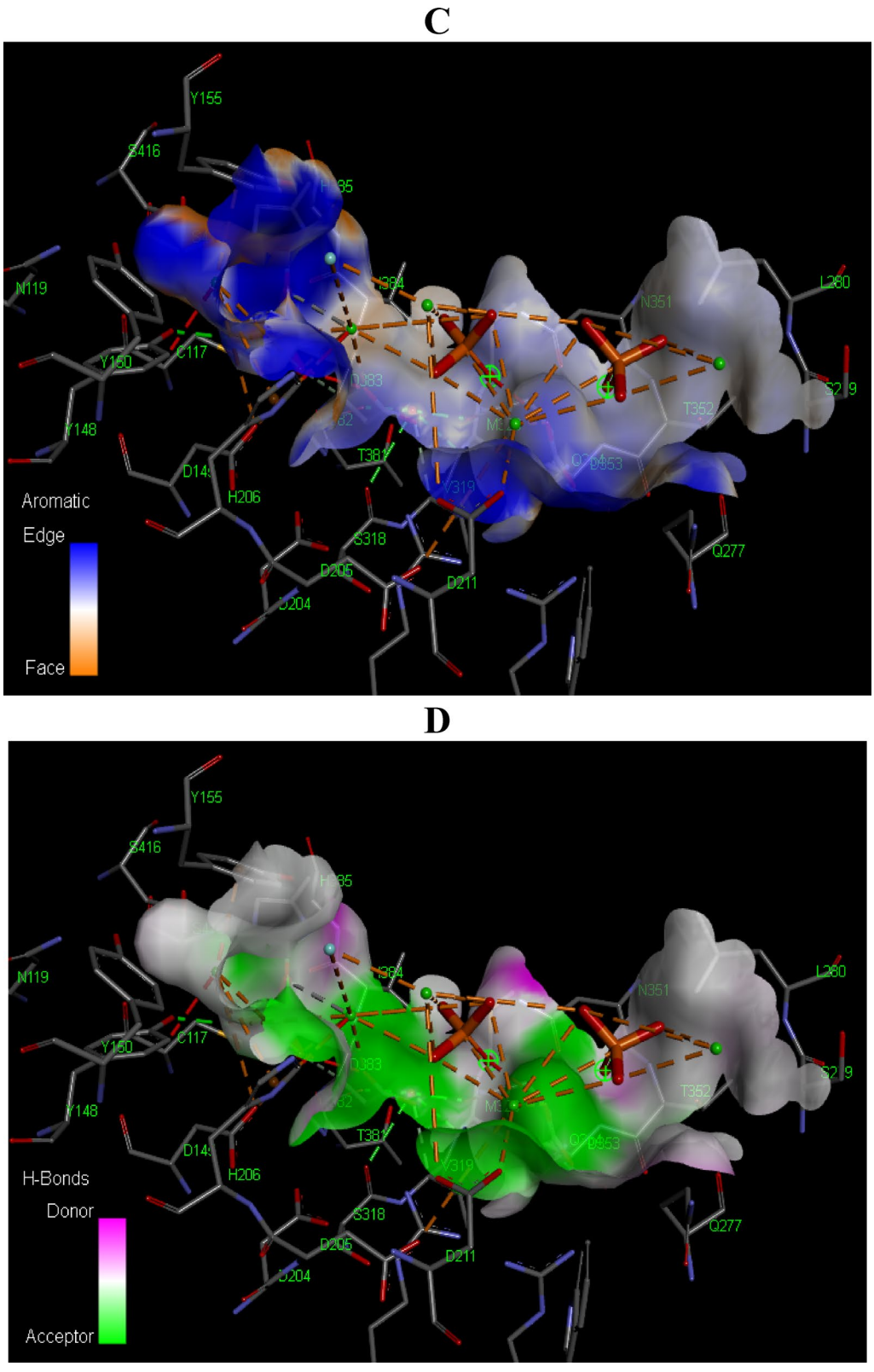

Fig. 7. (continued)

ACPase and *ALPase* expression

The *ACPase* and *ALPase* activity of *Streptomyces sp.* MMA-NRC was conducted by using a fermentation medium that was enhanced with 0.5% rock phosphate. The experiment included examining the *E. coli* recipient strains, the donor *Streptomyces sp.* MMA-NRC, and four *E. coli* strains harboring the *ACPase* and *ALPase* plasmids (*E.*

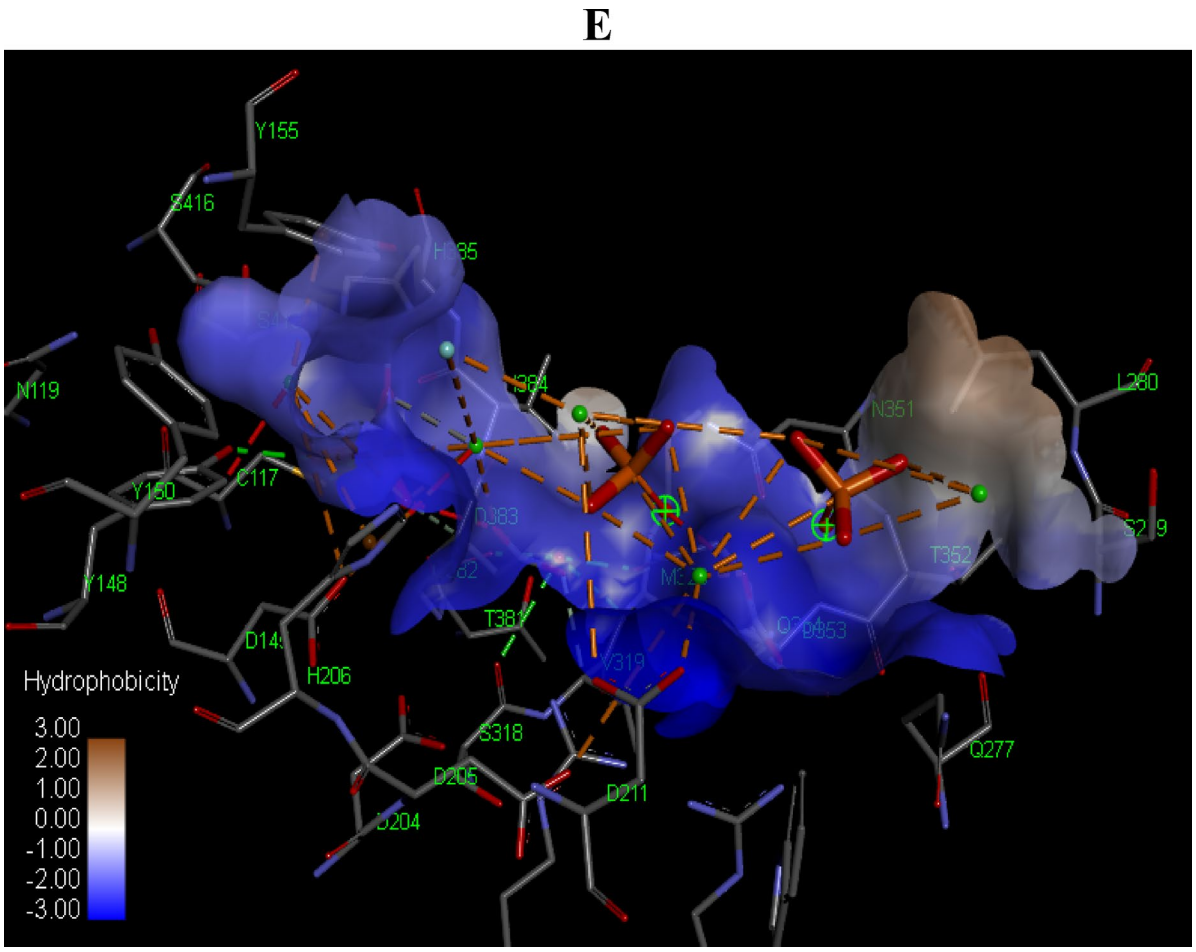

Fig. 7. (continued)

coli pGEM-T-ACPase and *E.coli pGEM-T-ALPase*). The cultures were placed in an incubator at a temperature of 37 °C and subjected to shaking at a speed of 120 revolutions per minute for a maximum duration of 7 days. Each culture was sampled and the obtained supernatant was obtained using centrifugation. This supernatant was used as the crude enzyme for the phosphatase activity test, following the previously described method. The findings revealed that the donor *Streptomyces sp.* MMA-NRC had *ACPase* and *ALPase* activity, but the recipient strains of *E. coli* showed no activity. Nevertheless, the *E. coli* cultures that obtained the *ACPase* and *ALPase* plasmids (*E. coli pGEM-T-ACPase* and *E. coli pGEM-T-ALPase*) exhibited *phosphatase* functionality. The results validated the biological functionality of the cloned *ACPase* and *ALPase* genes. Both *E. coli* recombinant strains exhibited *phosphatase* activity increase with the increase of incubation period with rock phosphate. The available phosphor was observed on seven day of incubation, with approximately pf 52.64 and 57.22 mg/L^{-1} for *E.coli* DH5α *pGEM-T-ACPase* and *E.coli* DH5α *pGEM-T-ALPase*, respectively, as shown in Fig. 8. In contrast, the wild-type *Streptomyces sp.* MMA-NRC displayed available phosphor of 35.44 mg/L^{-1} after 7 days of incubation, as reported by[17].

In a related study of[43], the recombinant plas mid pBL-ALP2 and empty vector pET19b were transformed to *E. coli* BL21 (DE3) for *APase* expression through induction with 0.5 mM IPTG at 37 °C for 3–4 h after the thermostatable *Alkaline Phosphatase APase* gene from *Bacillus licheniformis* MTCC 1483 was cloned into a His-tagged expression vector pET19b.A Ni-NTA affinity column was used to purify the recombinant enzyme, and the resultant enzyme had a specific activity of 24,890 U/mg protein.The enzyme demonstrated great thermostability and peak activity at pH 10.0 and 50 °C. In order to dephosphorylate linear DNA segments, the recombinant *alkaline phosphatase* from *B. licheniformis* MTCC 1483 demonstrated a dephosphorylation efficiency of 92.9%[44], reported *Escherichia coli* was cloned and shown to produce the *olpA* gene of *Chryseobacterium meningosepticum*, which codes for a molecular class C phosphatase. A 29-kDa polypeptide with an amino-terminal signal peptide characteristic of bacterial membrane lipoproteins is encoded by the gene. A functional product that primarily partitions in the outer membrane is the outcome of expression in *E. coli*. Two stages of ion exchange chromatography were used to purify a secreted soluble OlpA derivative (sOlpA) that was made in *E. coli* but lacked the N-terminal cysteine residue for lipid anchoring[45], after being cloned into the pET28(b) vector and overexpressed in *Escherichia coli* BL21 (DE3), the gene encoding M2-32, a non-specific *acid phosphatase*, was isolated. Size exclusion chromatography, dynamic light scattering, and sedimentation investigations showed a dimeric form of M2-32 in solution despite the monomeric form's molecular weight of about 28 kDa. Strong

a

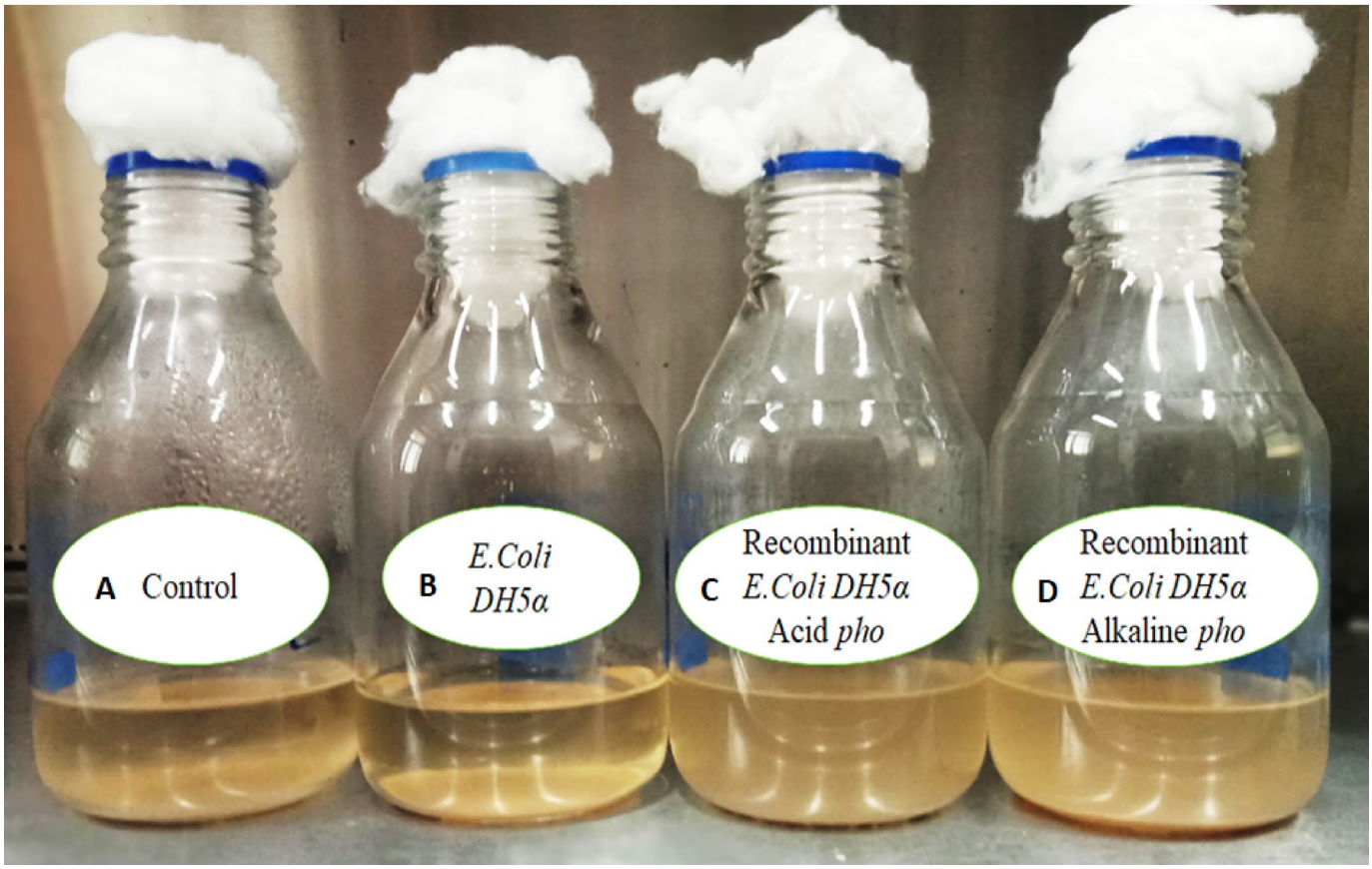

Fig. 8. rock phosphate solubilization of **(a)** control, **(b)***Ecoli DH5α*, **(c)** recombinant *Ecoli DH5α ACPase* and **(d)** recombinant *Ecoli DH5α ALPase* on NBRIP rock phosphate broth media without glucose addition after 7 days incubation.

activity was shown by enzymatic tests employing p-nitrophenyl phosphate, 4-methylumbelliferyl phosphate, and 3'- and 5'-adenosine monophosphate over a pH range of 4.0–8.0 at both 30 and 50 °C. The enzyme refolded following heat denaturation at 80 °C, despite differential scanning fluorimetry showing an unfolding temperature at 47 °C. In study[52], the gene encoding *alkaline phosphatase* from the psychrotrophic bacterium *Shewanella sp*. SIB1 was cloned, sequenced, and overexpressed in *Escherichia coli*.The recombinant protein was purified and its enzymatic properties were compared with those of *E. coli alkaline phosphatase* (*APase*), which shows an amino acid sequence identity of 37%. Additionally[53], demonstrated overexpressed the *phoK* gene from *Sphingomonas sp*., which codes for a new *alkaline phosphatase* called *PhoK*, in the radioresistant bacterium *Deinococcus radiodurans*. Using zymographic and enzyme activity tests, the resulting recombinant strain (Deino-PhoK) demonstrated exceptionally high *alkaline phosphatase* activity. Uranium may be precipitated effectively by Deino-PhoK cells across a broad range of input U values. The strain precipitated almost 90% of the uranium in 2 h at low uranyl concentrations (1 mM), and at 10 mM U concentration, it demonstrated a high loading capacity of approximately 10.7 g U/g of dry weight of cells[42], reported *Escherichia coli* strain BL21 (DE3) overexpressed the cloned *phoK* gene, which encodes the *alkaline phosphatase* from *Sphingomonas sp*. strain BSAR-1. Compared to BSAR-1, the resulting *E. coli* strain EK4 produced extracellular *PhoK* activity 13 times higher and overexpressed cellular activity 55 times higher[47], reported the existence of a putative *Acid Phosphatase* (AcpA; EC 3.1.3.2) was discovered through genomic sequence analysis of *Acinetobacter baumannii*. After creating a plasmid construct, *E. coli* showed high expression of the recombinant protein (*rAcpA*)[43], reported represent Asp73, Ser124, Thr177, Arg188, Glu344, Asp349, His353, Asp391, His392, and His434 in *E. coli* recombinant *APase*. With the exception of Ser124 and Arg188, which make up catalytic and phosphate-binding sites, respectively, the highly conserved residues form three metal-binding sites. Asp175 is a component of the Mg2+-binding site in *E. coli APase*, and its substitution with His, as in mammalian *APase*, increases the activity of the enzyme. Since Asp175 of *E. coli APase* is equivalent to His155 in recombinant *BlAPase*, this alteration may help raise the specific activity of recombinant *BlAPase* by improving its affinity for binding Mg^{2+}. Different sources have different amino acid residues that are closed to metal sites, which could lead to conformational modifications that alter the binding affinities of certain metal ions. The specific activity of recombinant *BlAPase* in the presence of metal ions may increase or decrease as a result of these conformational changes[54], reported *Streptomyces* isolate KT 6-4-1, *Streptomyces* isolate L3, *Bacillus* isolate MC 9 and *Streptomyces* isolate ST 3 rock Phosphate solubilization ability in PVK Broth of 37.59, 15.37, 5.96 and 30.98; respectively.

Conclusion

Due to the wide range of applications, phosphatase had attracted a lot of attention. *Streptomyces sp.* MMA-NRC, an actinomycetes strain, was isolated and identified as a potential strain for the production of the phosphatase enzyme. The unique *Streptomyces sp.* 4 F and *Streptomyces sp.* MMA-NRC, which encode *ACPase* and *ALPase* genes, were isolated, sequenced, and submitted to the NCBI GenBank accession number based on the conserved rejoin. The Ramachandran plot, which demonstrated that the residues were accurately modelled, was used to validate the 3D model. *Streptomyces sp.* MMA-NRC *ACPase* and *ALPase* ultimately exhibited a contact with a high affinity score, according to molecular docking experiments. *Streptomyces sp.* MMA-NRC *ACPase* and *ALPase* expressing genes that were effectively cloned and expressed in *E. coli DH5α*, yielding greatly elevated levels of phosphatase activity and available phosphorus. This study's findings highlight the promise of microbial phosphatase, especially *ACPase* and *ALPase*, for rock phosphate solubilization. Other agriculture that rock phosphate solubilization, such as plant growth promotion, may be good candidates for further investigation into the potential applications of *phosphatase*. In order to create sustainable cropping systems, *Streptomyces sp.* will therefore be promising at the same time that crop productivity and economic-environmental sustainability need to be chosen, characterised, and identified.

Data availability

The datasets generated and/or analyzed during the current study are available in the GenBank repository, [https://www.ncbi.nlm.nih.gov/nuccore/OR770185](https:/www.ncbi.nlm.nih.gov/nuccore/OR770185) , [https://www.ncbi.nlm.nih.gov/nuccore/ PV646716,](https:/www.ncbi.nlm.nih.gov/nuccore/%20PV646716,%20) [https://www.ncbi.nlm.nih.gov/nuccore/ PV646717,](https:/www.ncbi.nlm.nih.gov/nuccore/%20PV646717,%20%20).

Received: 28 August 2025; Accepted: 23 December 2025
Published online: 20 February 2026

References

1. Siedliska, A., Piotr, B., Joanna, P., Monika, Z. & Jaromir, K. Identification of plant leaf phosphorus content at different growth stages based on hyperspectral reflectance. *BMC Plant. Biol.* **21**, 28 (2021).
2. Elhaissoufi, W., Ghoulam, C., Barakat, A., Zeroual, Y. & Bargaz, A. Phosphate bacterial solubilization: A key rhizosphere driving force enabling higher P use efficiency and crop productivity. *J. Adv. Res.* **38**, 13–28 (2022).
3. Chouyia, F., Ventorino, V. & Pepe, O. Diversity, mechanisms and beneficial features of phosphate-solubilizing *Streptomyces* in sustainable agriculture: A review. *Front. Plant. Sci.* **13**, 1035358 (2022).
4. Alori, E., Glick, B. & Babalola, O. Microbial phosphorus solubilization and its potential for use in sustainable agriculture. *Front. Microbiol.* **8**, 971 (2017).
5. Suleimanova, A. D. et al. Novel glucose-1-phosphatase with high phytase activity and unusual metal ion activation from soil bacterium *pantoea sp.* strain 3.5.1. *Appl. Environ. Microbiol.* **81**, 6790–6799 (2015).
6. Santos, H. et al. *Bacillus velezensis* associated with organomineral fertilizer and reduced phosphate doses improves soil microbial—Chemical properties and biomass of sugarcane. *Agronomy* **12**, 2701 (2022).
7. Singh, A. et al. Understanding soil carbon and phosphorus dynamics under grass-legume intercropping in a semi-arid region. *Agronomy* **13**, 1692 (2023).
8. Ahmad, N. et al. Environmental implications of phosphate-based fertilizer industrial waste and its management practices. *Environ. Monit. Assess.* **195**, 1326 (2023).
9. Cordell, D., Schmid-Neset, T., White, S. & Drangert, J. O. Preferred future phosphorus scenarios: A framework for meeting long-term phosphorus needs for global food demand. In *Proceedings of the International Conference on Nutrient Recovery from Wastewater Streams, Vancouver, BC, Canada* 10–13 (2009).
10. Cooper, J., Lombardi, R., Boardman, D. & Carliell-Marquet, C. The future distribution and production of global phosphate rock reserves. *Resour. Conserv. Recycl.* **57**, 78–86 (2011).
11. Gross, A., Lin, Y., Weber, P. K., Pett-Ridge, J. & Silver, W. L. The role of soil redox conditions in microbial phosphorus cycling in humid tropical forests. *J. Ecol.* **101**, e02928 (2020).
12. Liang, J. et al. Novel phosphate-solubilizing bacteria enhance soil phosphorus cycling following ecological restoration of land degraded by mining. *ISME J.* **14**, 1600–1613 (2020).
13. Neal, A. et al. Phylogenetic distribution, biogeography and the effects of land management upon bacterial non-specific *acid phosphatase* gene diversity and abundance. *Plant. Soil.* **427**, 175–189 (2018).
14. Udaondo, Z. et al. Developing robust protein analysis profiles to identify bacterial *acid phosphatases* in genomes and metagenomic libraries. *Environ. Microbiol.* **22**, 3561–3571 (2020).
15. Kiprotich, K., Muoma, J., Omayio, D., Ndombi, T. & Wekesa, C. Molecular characterization and mineralizing potential of phosphorus solubilizing bacteria colonizing common bean (*Phaseolus vulgaris L.*) rhizosphere in Western Kenya. *Int. J. Microbiol.* **2023**, 6668097 (2023).
16. Massucato, L. et al. Efficiency of combining strains Ag87 (*Bacillus megaterium*) and Ag94 (*Lysinibacillus sp.*) as phosphate solubilizers and growth promoters in maize. *Microorganisms* **10**, 1401 (2020).
17. Abd El-Aziz, N. M. et al. Biosolubilization of rock phosphate by *Streptomyces sp*. MMA-NRC isolated from rhizospheric soil and assessment of ability on wheat growth promotion: insights from genetic improvement random mutation induction Approach, Egyptian academic. *J. Biol. Sci.* **16** (2), 49–79 (2024).
18. El-Kherbawy, M. I. et al. Chemical characterization of phosphate rock applied in arid region. *Middle East. J. Agric. Res.* **3** (1), 59–70 (2014).
19. Nautiyal, C. S. An efficient microbiological growth medium for screening phosphate solubilizing microorganisms. *FEMS Microbiol. Lett.* **170** (1), 265–270 (1999).
20. Murphy, J. & Riley. J. R A modified single solution method for the determination of phosphorus in natural waters. *Chem. Acta*. **27**, 31–36 (1962).
21. Olsen, S. R., Cole, C. V., Watanabe, F. S. & Dean, L. A. *Estimation of Available Phosphorus in Soils by Extraction with* $NaHCO_3$ (U.S., 1954).
22. Kumar, S., Stecher, G., Li, M., Knyaz, C. & Tamura, K. MEGA X: molecular evolutionary genetics analysis across computing platforms. *Mol. Biol. Evol.* **35** (6), 1547 (2018).
23. Mei, Y., Chen, Y., Zhai, R. & Liu, Y. Cloning, purification and biochemical properties of a thermostable pectinase from *Bacillus halodurans* M29. *J. Mol. Catal. B Enzym.* **94**, 77–81 (2013).

24. Eswar, N. et al. Comparative protein structure modeling using modeller. *Curr. Protoc. Bioinform.* (2006).
25. Yang, J. & Zhang, Y. I-TASSER server: new development for protein structure and function predictions. *Nucleic Acids Res.* **43** (W1), W174–W181 (2015).
26. Kathwate, G. H. In Silico design and characterization of multiepitopes vaccine for SARS-CoV2 from its Spike proteins. *BioRxiv* **56**, 1115–1135 (2020).
27. Heo, L., Park, H. & Seok, C. GalaxyRefne: protein structure refnement driven by side-chain repacking. *Nucleic Acids Res.* **41**, 384–388 (2013).
28. Sahi, S., Tewatia, P. & Malik, B. K. Modeling and simulation studies of human b3 adrenergic receptor and its interactions with agonists. *Curr. Comput. Aided Drug Des.* **8**, 283–295 (2012).
29. Singh, K. D. & Muthusamy, K. Molecular modeling, quantum polarized ligand Docking and structure-based 3D-QSAR analysis of the imidazole series as dual AT1 and ETA receptor antagonists. *Acta Pharmacol. Sin.* **34**, 1592–1606 (2013).
30. Patni, K., Agarwal, P., Kumar, A. & Meena, L. S. Computational evaluation of anticipated PE_PGRS39 protein involvement in host–pathogen interplay and its integration into vaccine development. *3 Biotech.* **11** (204), 1–17 (2021).
31. Beg, M. A., Shivangi, Thakur, S. C. & Meena, L. S. Structural prediction and mutational analysis of Rv3906c gene of *Mycobacterium tuberculosis* H37Rv to determine its essentiality in survival. *Adv. Bioinf.* **15**, 6152014 (2018).
32. Gupta, S., Tewatia, P., Misri, J. & Singh, R. Molecular modeling of cloned *Bacillus subtilis* keratinase and its insinuation in psoriasis treatment using Docking studies. *Indian J. Microbiol.* **57** (4), 485–491 (2017).
33. Degryse, B. et al. Silico Docking of urokinase plasminogen activator and integrins. *BMC Bioinform.* **9**, 1–9 (2008).
34. Banerjee, A. et al. Structural characterization and active site prediction of bacterial keratinase through molecular Docking. *J. Bioinform.* **4**, 67–82 (2014).
35. Sambrook, J. & Russell, D. W. *Molecular Cloning: A Laboratory Manual*, 3 edn. 132–150 (Cold Spring Harbor Laboratory Press, 2001).
36. Li, X. et al. An improved calcium chloride method preparation and transformation of competent cells. *Afr. J. Biotechnol.* **9** (50), 8549–8554 (2010).
37. Hanahan, D., Jessee, J. & Bloom, F. R. Plasmid transformation of *Escherichia coli* and other bacteria. *Methods Enzymol.* **20**, 63–113 (1991).
38. Barman, D. N., Haque, M. D. A., Islam, S. M. D. A., Yun, H. D. & Kim, M. K. Cloning and expression of *OphB* gene encoding organophosphorus hydrolase from endophytic *Pseudomonas sp*. BF1-3 degrades organophosphorus pesticide Chlorpyrifos. *Ecotoxicol. Environ. Saf.* **108**, 135–141 (2014).
39. Kesharwani, R. K. & Misra, K. Prediction of binding site for curcuminoids at human topoisomerase II a protein; an in Silico approach. *Curr. Sci.* **101**, 1060–1065 (2011).
40. Froger, A. & Hall, J. E. Transformation of plasmid DNA into *E. coli* using the heat shock method. *J. Vis. Exp.* **6**, 253 (2007).
41. Li, H., Li, R., Yu, H., Zhang, Y. & Feng, H. Evolution and classification of *Ser/Thr phosphatase* PP2C family in bacteria: sequence conservation, structures, domain distribution. *PLoS One.* **20** (5), e0322880 (2025).
42. Nilgiriwala, K. S., Alahari, A., Rao, A. S. & Apte, S. K. Cloning and overexpression of *alkaline phosphatase PhoK* from *Sphingomonas sp*. strain BSAR-1 for bioprecipitation of uranium from alkaline solutions. *Appl. Environ. Microbiol.* **74** (17), 5516–5523 (2008).
43. Divya, A., Santhiagu, A. & Jaya Prakash, S. Cloning, expression and characterization of a highly active thermostable *Alkaline phosphatase* from *Bacillus licheniformis* MTCC 1483 in *Escherichia coli* BL21 (DE3)1. *Appl. Biochem. Microbiol.* **52** (4), 358–365 (2016).
44. Passariello, C. et al. The molecular class C *acid phosphatase* of *Chryseobacterium meningosepticum* (*OlpA*) is a broad-spectrum nucleotidase with Preferential activity on 5'-nucleotides. *Biochim. Biophys. Acta.* **1648** (1–2), 203–209 (2003).
45. Recio, M. I. et al. Thermotolerant class A *acid phosphatase* active across broad pH range and diverse substrates. *Protein Sci.* **34** (9), e70244 (2025).
46. Martínez-Canseco, C. et al. Detection and expression of *SapS*, a class C nonspecific *acid phosphatase* with *O-phospho-Ltyrosine*-phosphatase activity, in *Staphylococcus aureus* isolates from patients with chronic osteomyelitis. *Biomedica* **43** (2), 200–212 (2023).
47. Smiley-Moreno, E. et al. Biochemical characterization of a recombinant *acid phosphatase* from *Acinetobacter baumannii*. *PLoS One.* **16** (6), e0252377 (2021).
48. Pramanik, K. et al. An insilico structural, functional and phylogenetic analysis with three dimensional protein modeling of *alkaline phosphatase* enzyme of *Pseudomonas aeruginosa*. *J. Genetic Eng. Biotechnol.* **15**, 527–537 (2017).
49. Gandhi, N. U. & Chandra, S. B. A. Comparative analysis of three classes of bacterial non-specific *Acid phosphatases* and *archaeal phosphoesterases*: evolutionary perspective. *Acta Inf. Med.* **20** (3), 167–173 (2012).
50. Sajeev-Sheeja, A. & Zhang, S. Structural molecular modeling of bacterial integral membrane protein enzymes and their AlphaFold2 predicted water-soluble QTY variants. *J. Proteins Proteom.* **15** (4), 635–645 (2024).
51. Caban-Penix, S., Ho, K., Yang, Z., Baral, R. & Bradshaw, N. Docking interactions determine substrate specificity of members of a widespread family of protein phosphatases. *J. Biol. Chem.* **300** (9), 107700 (2024).
52. Yutaka, S. et al. Gene cloning, overproduction, and characterization of thermolabile *Alkaline Phosphatase* from a *Psychrotrophic* Bacterium. *Biosci. Biotechnol. Biochem.* **69** (2), 364–373 (2005).
53. Kulkarni, S., Ballal, A. & Apte, S. K. Bioprecipitation of uranium from alkaline waste solutions using Recombinant *Deinococcus Radiodurans*. *J. Hazard. Mater.* **262**, 853–861 (2013).
54. Chaiharn, M., Pathom-aree, W., Sujada, N. & Lumyong, S. Characterization of phosphate solubilizing *Streptomyces* as a biofertilizer. *Chiang Mai J. Sci.* **45** (2), 701–716 (2018).

Acknowledgements

Thank you.

Author contributions

Author executed the experimental procedures and planned the study technique. Writing, editing, and revision of articles in addition to data analysis and illustration, prepared the figures and read the manuscript's corresponding parts.

Funding

Open access funding provided by The Science, Technology & Innovation Funding Authority (STDF) in cooperation with The Egyptian Knowledge Bank (EKB).

Declarations

Competing interests

The authors declare no competing interests.

Additional information

Correspondence and requests for materials should be addressed to N.M.A.-A.